

# Structure-Aware Matrix Pencil Method

Yehonatan-Itay Segman<sup>1</sup>, Alon Amar<sup>1</sup> and Ronen Talmon<sup>1</sup>

<sup>1</sup>Viterbi Faculty of Electrical and Computer Engineering,  
Technion - Israel Institute of Technology, Haifa 32000, Israel.  
yehonatans@campus.technion.ac.il, aamar@technion.ac.il, ronon@ef.technion.ac.il

**Abstract**—We address the problem of detecting the number of complex exponentials and estimating their parameters from a noisy signal using the Matrix Pencil (MP) method. We introduce the MP *modes* and present their informative spectral structure. We show theoretically that these modes can be divided into signal and noise modes, where the signal modes exhibit a perturbed Vandermonde structure. Leveraging this structure, we proposed a new MP algorithm, termed the SAMP algorithm, which has two novel components. First, we present a new and robust model order detection with theoretical guarantees. Second, we present an efficient estimation of signal amplitudes. We show empirically that the SAMP algorithm significantly outperforms the standard MP method, particularly in challenging conditions with closely-spaced frequencies and low Signal-to-Noise Ratio (SNR) values, approaching the Cramer-Rao lower bound (CRB) for a broad SNR range. Additionally, compared with prevalent information-based criteria, we show that SAMP is more computationally efficient and insensitive to noise distribution.

**Index Terms**—Matrix Pencil Method, model order detection, Parameter estimation, closely-spaced frequencies, super-resolution.

## I. INTRODUCTION

Consider the classical model of a discrete-time signal consisting of a sum of complex exponentials and additive noise:

$$y(n) = x(n) + w(n), \quad (1)$$

where  $0 \leq n \leq N - 1$ ,  $w(n)$  is the additive noise, and  $x(n)$  is the signal term expressed as a finite sum of complex exponentials given by:

$$x(n) = \sum_{i=1}^M b_i e^{(-\alpha_i + j\theta_i)n}, \quad (2)$$

where  $M$  is the number of complex exponentials (or model order),  $b_i = |b_i|e^{j\phi_i}$  are the complex amplitudes,  $\phi_i \in \mathbb{R}$  are the initial phases,  $\alpha_i \in \mathbb{R}$  are the (non-negative) damping factors,  $\theta_i \in \mathbb{R}$  are the normalized frequencies, and the lower case letter ‘j’ is the complex number  $j = \sqrt{-1}$ . The complex exponentials  $e^{-\alpha_i + j\theta_i}$  are conventionally represented as  $z_i = e^{-\alpha_i + j\theta_i}$ , and referred to as the signal poles. The signal poles are assumed to be distinct. Given the finite interval of  $N$  samples of  $y(n)$ , the goal is twofold: (i) detect the (discrete-valued) model order  $M$  (a detection step), and (ii) determine the (continuous-valued) parameters of interest (an estimation step), i.e.,  $\{b_i\}_{i=1}^M$ ,  $\{\alpha_i\}_{i=1}^M$ , and  $\{\theta_i\}_{i=1}^M$ .

This is a longstanding fundamental detection-estimation problem in signal processing, with a broad variety of applications in telecommunications, audio processing, radar systems, and biomedical signal analysis [1]–[3]. Over the years, numerous methods have been proposed, including maximum likelihood-based techniques [4]–[6], super-resolution pseudo-spectrum approaches such as Minimum Variance Distortionless Response (MVDR) (known also as Capon’s method) [7], Multiple Signal Classification (MUSIC) [8], Estimation of Signal Parameters via Rotational Invariant Techniques (ES-PRIT) [9], Method Of Direction Estimation (MODE) [10], Sparse Iterative Covariance-based Estimation (SPICE) [11], sparse model-based methods [12]–[18], optimization-based techniques [19], [20], and more recently, neural network-based approaches [21]–[27].

One common approach for such problems is based on information measures such as the Akaike Information Criterion (AIC), Bayesian Information Criterion (BIC), or Minimum Description Length (MDL) [1], [3]. In this approach, the detection and estimation steps are *coupled*; for each hypothesized model order, the most likely parameters are estimated. Despite its popularity and widespread use, this coupled approach has two main drawbacks. (i) It necessitates the computation of the likelihood function, which is usually unknown in practice. (ii) It is computationally demanding, as it involves repeated model parameter estimations for each hypothesized model order.

More computationally efficient is a *decoupled detection and estimation* approach, where the model order is determined first, followed by parameter estimation. A common *non-parametric* method involves computing a spectrum (or pseudo-spectrum) of the observations. For example, the model order can be determined by counting the number of significant peaks in the periodogram (or even Bartlett’s or Welch’s spectrum). This efficiency comes at the expense of two prominent limitations: limited frequency resolution, which is proportional to the reciprocal of the data length, and tapering / windowing effects [28]. These limitations pose significant concerns for short time series, and many alternatives have been proposed over the years to mitigate them.

Herein, we consider the *decoupled detection and estimation* approach and focus on the MP method, introduced by Hua and Sarkar in [29], as a super-resolution method. The MP method estimates the frequencies of superimposed complex exponentials by solving a generalized eigenvalue problem derived from the signal’s Hankel matrix. Consequently, compared to the classical Fourier analysis, it is not restricted to a specific regular grid and does not have a separation limit due to

tapering. The MP method has gained considerable attention for its superiority over other linear methods, such as Prony-based methods, demonstrating robustness to noise and computational efficiency [30], [31].

Several modifications to the MP algorithm that mitigate its sensitivity to additive white noise have been proposed in the literature including the Forward-Backward MP (FBMP) approach [30], [31] which is limited to undamped exponentials, the Band-Pass MP (BPMP), which is effective in the case of damped exponentials though its implementation requires prior knowledge of the signal and increased computation time [32], the Total-Least-Squares MP (TLS-MP) approach, which uses a pre-filtering step for noise mitigation [31], and the Total Forward-Backward MP (TFBMP), which surpasses the Fast Fourier Transform (FFT) in variance estimates beyond a specific SNR threshold, at the expense of a larger bias [33].

The above variations of the MP method first determine the model order of the problem through singular values truncation, then estimate the poles from the generalized eigenvalues, and finally estimate the amplitudes by solving a linear least square problem [31]. Additionally, the main theoretical result, introduced in [29, Theorem 2.1], only addresses noiseless scenarios, whereas noise is almost always present in real-world applications. The discrepancy between the ideal noiseless scenario in theory and the presence of noise in practice highlights the need to extend the MP theory to accommodate noisy signals.

In this paper, we present a new MP method, termed the Structure-Aware Matrix Pencil (SAMP), which implements a new strategy of “first estimate and then detect”, rather than the standard “detect and then estimate” approach. Our new method has two novel components: (i) a new approach for model order detection, and (ii) an efficient amplitude estimation. At the core of our method lie the MP *modes*, a new notion that is borrowed from the realm of dynamic mode decomposition (DMD) [34] and introduced in this context for the first time to the best of our knowledge. Concretely, the left and right MP *modes* are defined as the columns and rows of the pseudo-inverse matrix of the generalized eigenvectors matrix obtained by the MP method, respectively. We show theoretically that these MP modes can be divided into signal modes and noise modes, where the signal modes exhibit a perturbed Vandermonde structure. We theoretically study this perturbation and explicitly present the dependency on the model parameters. We put special focus on the impact of noise and extend the classical MP theorem in [29] to address noisy scenarios and demonstrate that all the signal components in (2) can be detected through the signal modes. Leveraging the structure of the signal modes, we depart from singular values thresholding heuristics. Instead, we propose a new model order detection with theoretical guarantees that depend on the SNR and the separation of the poles. We show empirically that the new SAMP algorithm obtains superior performance, particularly in challenging conditions with closely-spaced frequencies and low SNR values, compared with the standard MP method that is based on singular values heuristics for the model order detection. In addition, we show that compared with the prevalent MDL and AIC criteria, SAMP is insensitive to noise

distribution and is more computationally efficient.

The paper is organized as follows. In Sec. II we describe the existing MP method. In Sec. III we introduce the MP modes and analyze their structure. In Sec. IV we propose a novel order detection rule based on the MP modes structure. In Sec. V we proposed an efficient method for estimating the signal amplitudes using the MP modes. In Sec. VI we present the SAMP algorithm for estimating the model parameters. In Sec. VII we present simulation results. Finally, in Sec. VIII we summarize this paper with conclusions and discussion regarding possible practical implications and future research.

## II. THE CLASSICAL MATRIX PENCIL METHOD

The MP method estimates signal parameters by solving a generalized eigenvalue problem based on the available data samples. It begins by constructing an  $(N - L) \times (L + 1)$  Hankel matrix  $\mathbf{Y}$  from the noisy measurements  $y(n)$ :

$$\mathbf{Y} = \begin{bmatrix} y(0) & y(1) & \cdots & y(L) \\ y(1) & y(2) & \cdots & y(L+1) \\ \vdots & \vdots & \ddots & \vdots \\ y(N-L-1) & y(N-L) & \cdots & y(N-1) \end{bmatrix}. \quad (3)$$

The parameter  $L$ , termed the *pencil parameter*, is chosen to satisfy  $M \leq L \leq N - M$  (see sec. II-C for more details). Using perturbation analysis, it was demonstrated that the optimal range for minimizing variance in the estimator is  $\frac{N}{3} \leq L \leq \frac{N}{2}$  [29], [30], [35]–[37]. For the rest of this paper, we assume that  $L$  lies within this optimal range.

Next, two sub-matrices  $\mathbf{Y}_0$  and  $\mathbf{Y}_1$  are formed from  $\mathbf{Y}$  by removing its last and first columns, respectively. A denoising step (see section II-A) is then performed using the singular value decomposition (SVD) of the Hankel matrix  $\mathbf{Y}_0$ :

$$\mathbf{Y}_0 = \mathbf{U}\mathbf{\Sigma}\mathbf{V}^H, \quad (4)$$

where  $\mathbf{U} \in \mathbb{C}^{(N-L) \times L}$  and  $\mathbf{V} \in \mathbb{C}^{L \times L}$  are unitary matrices,  $\mathbf{\Sigma} = \text{diag}(\sigma_1, \dots, \sigma_L)$  with  $\sigma_1 \geq \sigma_2 \geq \dots \geq \sigma_L$ , and  $(\cdot)^H$  denotes the complex conjugate transpose.

Using (4) we can express the MP by:

$$\mathbf{Y}_1 - \tilde{\lambda}\mathbf{Y}_0 = \mathbf{U}\mathbf{\Sigma}(\mathbf{A} - \tilde{\lambda}\mathbf{I})\mathbf{V}^H, \quad (5)$$

where the square, non-symmetric,  $L \times L$  matrix  $\mathbf{A}$  is given by:

$$\mathbf{A} = \mathbf{\Sigma}^{-1}\mathbf{U}^H\mathbf{Y}_1\mathbf{V}, \quad (6)$$

and we use the notation of  $\tilde{\lambda}$  to denote a perturbation of  $\lambda$ , an eigenvalue of the noiseless MP (see Section II-C for more details). The MP method is based on finding the eigenvalues of the MP  $\mathbf{Y}_1 - \tilde{\lambda}\mathbf{Y}_0$  as an estimate for the signal poles  $z_i$ . Instead of directly computing the eigenvalues of  $\mathbf{Y}_1 - \tilde{\lambda}\mathbf{Y}_0$ , the estimates of the signal poles are obtained by the eigenvalues of  $\mathbf{A}$  [29]. Accordingly, an eigenvalue decomposition (EVD) of the matrix  $\mathbf{A}$  is performed:

$$\mathbf{A} = \mathbf{Q}\tilde{\mathbf{\Lambda}}\mathbf{Q}^{-1}, \quad (7)$$

where  $\tilde{\mathbf{\Lambda}} = \text{diag}(\tilde{\lambda}_1, \dots, \tilde{\lambda}_L)$  and  $\mathbf{Q} \in \mathbb{C}^{L \times L}$  contains the eigenvectors as columns.

A critical problem arises as the matrices  $\mathbf{Y}_0$  and  $\mathbf{Y}_1$  have a full rank (which equals  $L$ ) stemming from the additive noise contamination. Consequently, the matrix  $\mathbf{A}$  has  $L$  non-zero eigenvalues, consisting of  $M$  signal-related eigenvalues, and  $L - M$  extraneous eigenvalues, containing only noise-related information [31]. Therefore, the model order (the number of complex exponentials) needs to be determined in addition to, and usually before, the estimation of the parameters.

#### A. Model order detection

Determining the model order in the MP method involves truncating the singular values from the SVD of  $\mathbf{Y}_0$  in (4), and the standard approach for this step is the decoupled detection-estimation approach. A commonly used technique is the Significant Decimal Digit (SDD) [29]–[31], [38], [39], where the model order is estimated by:

$$\widehat{M}_{\text{SD}} = \arg \min_{i=1, \dots, L} \{\sigma_i : \sigma_i / \sigma_{\max} \geq 10^{-p}\}, \quad (8)$$

where  $p$  is defined as the number of significant decimal digits in the data,  $\sigma_{\max}$  is the maximal singular value, and the singular values are assumed to be in descending order. Another closely related technique is the “gap” technique [33], [40], where the model order is estimated by:

$$\widehat{M}_{\text{GAP}} = \arg \max_{i=1, \dots, L-1} \{\sigma_i / \sigma_{i+1}\} \quad (9)$$

Although less mentioned in the MP literature, it is also possible to adopt the coupled detection-estimation approach. For example, consider the AIC criterion (similarly, the MDL criterion can be used), which is expressed as [3, Appendix C]:

$$\text{AIC}(k) = -2 \log(p_k(\mathbf{y} | \hat{\mathbf{v}}_k)) + 2k, \quad (10)$$

where  $\mathbf{y} = \{y(n)\}_{n=0}^{N-1}$  is the vector of observations (1), and  $p_k(\mathbf{y} | \hat{\mathbf{v}}_k)$  is the probability density function (PDF) of  $\mathbf{y}$  under the estimated parameter vector  $\hat{\mathbf{v}}_k$ , assuming the model order is  $k$ . Here, the estimated parameter vector is  $\hat{\mathbf{v}}_k = [\{\hat{b}_i\}_{i=1}^k, \{\hat{\alpha}_i\}_{i=1}^k, \{\hat{\theta}_i\}_{i=1}^k]$ . The estimated parameter vector is obtained using the MP method, and the model order is estimated by:

$$\widehat{M}_{\text{AIC}} = \arg \min_{k=1, \dots, M_{\max}} \{\text{AIC}(k)\}, \quad (11)$$

where  $M_{\max}$  is the maximum number of hypothesized exponentials (naturally,  $M_{\max} \leq L$ ).

**Remark 1.** *The coupled detection-estimation approach relies on computing the likelihood function, which requires prior knowledge of the noise distribution. In addition, it is computationally inefficient, as the likelihood must be calculated repeatedly for every possible hypothesized model order.*

#### B. Parameter estimation

Once we determine the model order  $\widehat{M}$ , we truncate the SVD of  $\mathbf{Y}_0$  in (4) to rank  $\widehat{M}$  and use the eigenvalues of the resulting  $\widehat{M} \times \widehat{M}$  matrix  $\mathbf{A}$  in (7) to estimate the signal poles.

The estimated damping factor and normalized frequency are given by:

$$\hat{\alpha}_i = \log|\tilde{\lambda}_i|, \quad \hat{\theta}_i = \arg(\tilde{\lambda}_i), \quad i = 1, 2, \dots, \widehat{M} \quad (12)$$

Next, the amplitudes  $\{b_i\}_{i=1}^{\widehat{M}}$  are estimated by solving the linear least squares problem [31]:

$$\hat{b}_i = \arg \min_{b_i} \sum_{n=0}^{N-1} |y(n) - \tilde{\lambda}_i^n b_i|^2, \quad (13)$$

which has a closed-form solution of:

$$\hat{\mathbf{b}} = \begin{bmatrix} 1 & 1 & \dots & 1 \\ \tilde{\lambda}_1 & \tilde{\lambda}_2 & \dots & \tilde{\lambda}_{\widehat{M}} \\ \tilde{\lambda}_1^2 & \tilde{\lambda}_2^2 & \dots & \tilde{\lambda}_{\widehat{M}}^2 \\ \vdots & \vdots & \ddots & \vdots \\ \tilde{\lambda}_1^{N-1} & \tilde{\lambda}_2^{N-1} & \dots & \tilde{\lambda}_{\widehat{M}}^{N-1} \end{bmatrix}^\dagger \begin{bmatrix} y(0) \\ y(1) \\ y(2) \\ \vdots \\ y(N-1) \end{bmatrix}, \quad (14)$$

where  $(\cdot)^\dagger$  denotes the pseudo-inverse and

$$\hat{\mathbf{b}} = [\hat{b}_1, \hat{b}_2, \dots, \hat{b}_{\widehat{M}}]^T \in \mathbb{C}^{\widehat{M}}.$$

#### C. The degenerate noiseless case

In the noiseless case, Hua et al. presented a complete theorem [29, Theorem 2.1], showing that the signal can be fully characterized using the noiseless MP solutions. Specifically, if  $M \leq L \leq N - M$ , the solutions  $(\lambda, \mathbf{q}, \mathbf{p}^H)$  to the generalized noiseless eigenvalue problem:

$$(\mathbf{X}_1 - \lambda \mathbf{X}_0) \mathbf{q} = 0, \quad \mathbf{p}^H (\mathbf{X}_1 - \lambda \mathbf{X}_0) = 0, \quad (15)$$

such that  $\mathbf{q} \in \text{Range}(\mathbf{X}_0^H)$  and  $\mathbf{p} \in \text{Range}(\mathbf{X}_0)$  are  $(z_i, \mathbf{q}_i, \mathbf{p}_i^H)$ , where  $\mathbf{q}_i$  is the  $i$ -th column of

$$\mathbf{Z}_R^\dagger = \mathbf{Z}_R^H (\mathbf{Z}_R \mathbf{Z}_R^H)^{-1},$$

$\mathbf{p}_i^H$  is the  $i$ -th row of

$$\mathbf{Z}_L^\dagger = (\mathbf{Z}_L^H \mathbf{Z}_L)^{-1} \mathbf{Z}_L^H,$$

and:

1)  $\mathbf{Z}_L \in \mathbb{C}^{(N-L) \times M}$  is a Vandermonde matrix given by:

$$\begin{bmatrix} 1 & 1 & \dots & 1 \\ z_1 & z_2 & \dots & z_M \\ z_1^2 & z_2^2 & \dots & z_M^2 \\ \vdots & \vdots & \ddots & \vdots \\ z_1^{N-L-1} & z_2^{N-L-1} & \dots & z_M^{N-L-1} \end{bmatrix}. \quad (16)$$

2)  $\mathbf{Z}_R \in \mathbb{C}^{M \times L}$  is a Vandermonde matrix given by:

$$\begin{bmatrix} 1 & z_1 & z_1^2 & \dots & z_1^{L-1} \\ 1 & z_2 & z_2^2 & \dots & z_2^{L-1} \\ \vdots & \vdots & \vdots & \ddots & \vdots \\ 1 & z_M & z_M^2 & \dots & z_M^{L-1} \end{bmatrix}. \quad (17)$$

The theorem is based on the following Vandermonde factorization of the noiseless Hankel matrices:

$$\begin{aligned} \mathbf{X}_0 &= \mathbf{Z}_L \mathbf{B} \mathbf{Z}_R, \\ \mathbf{X}_1 &= \mathbf{Z}_L \mathbf{B} \mathbf{Z} \mathbf{Z}_R, \end{aligned} \quad (18)$$

where  $\mathbf{B}$  and  $\mathbf{Z}$  are  $M \times M$  diagonal matrices comprising the signal's amplitudes and poles, respectively. For the proof and more details, see [29, Theorem 2.1].

As noted in [29], left-multiplying (15) by  $\mathbf{X}_0^\dagger$ , implies that the non-zero eigenvalues of the matrix  $\mathbf{X}_0^\dagger \mathbf{X}_1 \in \mathbb{C}^{L \times L}$  are precisely the  $M$  signal poles,  $\{z_i\}_{i=1}^M$ . Furthermore, since the matrix  $\mathbf{X}_0^\dagger \mathbf{X}_1 = \mathbf{Z}_R^\dagger \mathbf{Z} \mathbf{Z}_R$  has a rank of  $M \leq L$ , it also has  $L - M$  zero eigenvalues with corresponding right eigenvectors in the null space of  $\mathbf{Z}_R$ .

While the MP theorem only addresses noiseless scenarios, practical situations involve noisy measurements. The impact of noise is substantial and current literature is built upon thresholding techniques of singular values, as discussed in II-A. However, in cases of closely-spaced frequencies and low SNR values, these techniques tend to under-estimate or over-estimate the model order  $M$  (See Section VII). In Section III, we introduce the MP *modes*, which are derived by accounting for noise effects, and reveal the spectral structure of the signal-related modes. This structure allows us to identify the signal-related modes and estimate  $M$  more accurately (see Section VI), eliminating the need for singular values thresholding heuristics that are usually employed in the decoupled approach.

### III. INTRODUCING THE MP MODES

The traditional model order detection in the MP method relies on the SVD of  $\mathbf{Y}_0 = \mathbf{U} \mathbf{\Sigma} \mathbf{V}^H$ , given in (4). However, we now demonstrate that  $\mathbf{Y}_0$  can be further decomposed into a product of matrices, and the structure of these matrices can be leveraged to determine the model order. Recall that, in the noiseless case, the factorization in (18) consists of the matrices  $\mathbf{Z}_R$  and  $\mathbf{Z}_L$ , which are (i) Vandermonde matrices, and (ii) the pseudo-inverses of the right and left eigenvector matrices of the noiseless MP  $\mathbf{X}_1 - \lambda \mathbf{X}_0$ . To introduce a similar factorization in the noisy case, we first define the noisy counterparts of  $\mathbf{Z}_R$  and  $\mathbf{Z}_L$  using the SVD of  $\mathbf{Y}_0$  from (4), as the MP *modes*:

**Definition 1** (MP modes). *Define the right MP modes as the rows of:*

$$\tilde{\mathbf{Z}}_R := \mathbf{Q}^{-1} \mathbf{V}^H \in \mathbb{C}^{L \times L}. \quad (19)$$

*Similarly, define the left MP modes as the columns of:*

$$\tilde{\mathbf{Z}}_L := \mathbf{U} \mathbf{\Sigma} \mathbf{Q} \in \mathbb{C}^{(N-L) \times L}. \quad (20)$$

We note that the notion of “modes” is borrowed from the related DMD approach [41, Chap. 1] and, in the context of the MP method, it is new. In the sequel, we demonstrate that these modes contain spectral information that can be utilized in the detection step. These matrices, are the pseudo-inverses of the right and left eigenvector matrices of the noisy MP  $\mathbf{Y}_1 - \lambda \mathbf{Y}_0$ , given according to (5) and (7) by:

$$\tilde{\mathbf{Z}}_R^\dagger = \mathbf{V} \mathbf{Q}, \quad (21)$$

$$\tilde{\mathbf{Z}}_L^\dagger = \mathbf{Q}^{-1} \mathbf{\Sigma}^{-1} \mathbf{U}^H, \quad (22)$$

respectively. By normalizing  $\tilde{\mathbf{Z}}_R$  and  $\tilde{\mathbf{Z}}_L$  (See Appendix B in the Supplementary Materials (SM))<sup>1</sup> and combining them with

<sup>1</sup>For simplicity, we do not introduce a new notation for the normalized modes.

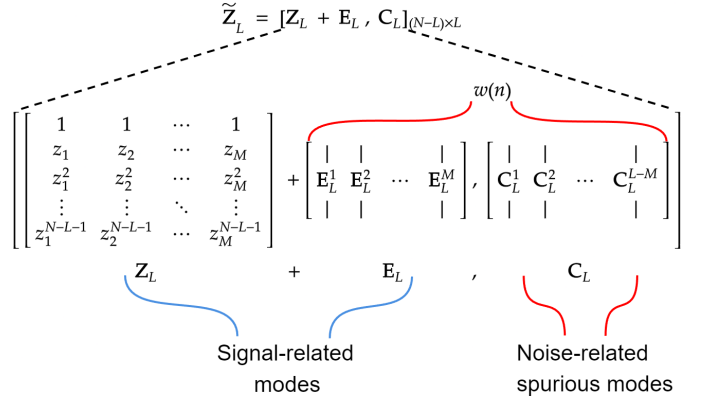


Fig. 1: The structure of  $\tilde{\mathbf{Z}}_L$  by Proposition 1. The matrices  $\mathbf{E}_L$  and  $\mathbf{C}_L$  are a direct result of the additive noise  $w(n)$ .

the SVD of  $\mathbf{Y}_0$ , we can express the data matrices  $\mathbf{Y}_0$  and  $\mathbf{Y}_1$  as follows:

$$\begin{aligned} \mathbf{Y}_0 &= \tilde{\mathbf{Z}}_L \tilde{\mathbf{B}} \tilde{\mathbf{Z}}_R, \\ \mathbf{Y}_1 &= \tilde{\mathbf{Z}}_L \tilde{\mathbf{B}} \tilde{\mathbf{\Lambda}} \tilde{\mathbf{Z}}_R, \end{aligned} \quad (23)$$

where  $\tilde{\mathbf{B}}, \tilde{\mathbf{\Lambda}} \in \mathbb{C}^{L \times L}$  are diagonal matrices containing the noisy amplitudes and poles, respectively. This decomposition forms a noisy analogous to the decomposition of  $\mathbf{X}_0$  and  $\mathbf{X}_1$  in (18). For more details see Appendix B in the SM, where we provide a comprehensive theorem that establishes the extension of the classical MP theorem to accommodate signals contaminated by noise. The next result shows that  $\tilde{\mathbf{Z}}_L$  has a valuable structure (a similar argument applies to  $\tilde{\mathbf{Z}}_R$ , but is omitted for brevity).

**Proposition 1.** *The matrix  $\tilde{\mathbf{Z}}_L$  (20), whose columns are the left MP modes, can be recast as*

$$\tilde{\mathbf{Z}}_L = [\mathbf{Z}_L + \mathbf{E}_L, \mathbf{C}_L]_{(N-L) \times L}, \quad (24)$$

where the  $M$  leftmost columns of  $\tilde{\mathbf{Z}}_L$  are the sum of the Vandermonde matrix  $\mathbf{Z}_L \in \mathbb{C}^{(N-L) \times M}$  and a noise-related component, denoted by  $\mathbf{E}_L \in \mathbb{C}^{(N-L) \times M}$ . The remaining  $L - M$  columns are noise-related spurious columns, denoted by  $\mathbf{C}_L \in \mathbb{C}^{(N-L) \times (L-M)}$ .

*Proof.* See Appendix B in the SM.  $\square$

*Signal and noise modes:* in the noiseless case, the matrix  $\mathbf{Z}_L$  assumes a Vandermonde structure (16). In the noisy case, by (24), the matrix  $\tilde{\mathbf{Z}}_L$  can be divided into two sub-matrices: the signal-related sub-matrix comprising the *signal modes*, represented by the  $M$  leftmost columns  $\mathbf{Z}_L + \mathbf{E}_L$ , and the noise-related sub-matrix comprising the *noise modes*, represented by the  $L - M$  rightmost columns  $\mathbf{C}_L$ . In addition, each signal mode is a column of a Vandermonde matrix associated with a signal pole, obscured by the additive noise term  $\mathbf{E}_L$ . See Fig. 1 for illustration.

Critically, Proposition 1 is meaningful and has a practical value only when the noise term  $\mathbf{E}_L$  has a structure that allows accurate extraction of the Vandermonde structure. Therefore, in the sequel, we analyze the noise matrix  $\mathbf{E}_L$ . The analysis of  $\mathbf{E}_R$  follows similarly and is therefore omitted.

### A. Analysis of the noise induced matrix

The analysis of  $\mathbf{E}_L$  is based on the analysis of the matrix  $\mathbf{Y}_0^\dagger \mathbf{Y}_1$  as a perturbation of the matrix  $\mathbf{X}_0^\dagger \mathbf{X}_1$ , denoted by:

$$\mathbf{Y}_0^\dagger \mathbf{Y}_1 = \mathbf{X}_0^\dagger \mathbf{X}_1 + \delta(\mathbf{X}_0^\dagger \mathbf{X}_1). \quad (25)$$

Since the matrix  $\mathbf{X}_0^\dagger \mathbf{X}_1$  has exactly  $M$  distinct non-zero eigenvalues and another  $L - M$  zero eigenvalues, the Rank-Nullity Theorem guarantees that its eigenvectors form a basis. Let  $\mathbf{T}_L^H(\mathbf{X}_0^\dagger \mathbf{X}_1)\mathbf{T}_R = \mathbf{\Lambda}$  be the eigenvalue decomposition of  $\mathbf{X}_0^\dagger \mathbf{X}_1$ , where  $\mathbf{\Lambda}$  is a diagonal matrix consisting of the eigenvalues  $\{\lambda_k\}_{k=1}^L$ , and  $\mathbf{T}_L$  and  $\mathbf{T}_R$  consist of the complete sets of left and right eigenvectors,  $\{\mathbf{p}'_k\}_{k=1}^L$  and  $\{\mathbf{q}'_k\}_{k=1}^L$ , respectively, with  $\mathbf{p}'_k \mathbf{q}'_k = 0$  for  $k \neq i$ . Without loss of generality, suppose that the eigenvalues  $\{\lambda_i\}_{i=1}^M$  are non-zero, simple, and equal the signal poles  $\{z_i\}_{i=1}^M$ , as guaranteed in the MP theorem for the noiseless case described in Section II-C.

For a simple eigenvector  $\mathbf{q}'_i$ , let  $\tilde{\mathbf{q}}'_i$  be its analogous perturbed eigenvector, which is an eigenvector of  $\mathbf{Y}_0^\dagger \mathbf{Y}_1$  (see proof of Lemma 1 in Appendix A, for more details). Appropriate normalization of these eigenvectors is essential for the subsequent theoretical results, which is formulated in the following assumption.

**Assumption 1.** For  $1 \leq i \leq M$ , we assume that  $\mathbf{p}'_i \tilde{\mathbf{q}}'_i = 1$ .

We remark that other alternative normalizations of  $\tilde{\mathbf{q}}'_i$ , such as  $\tilde{\mathbf{q}}'_i \tilde{\mathbf{q}}'_i = 1$  or  $\mathbf{q}'_i \tilde{\mathbf{q}}'_i = 1$ , are mentioned in the literature [42]. However, using such normalization will lead, in the sequel, to significant numerical errors due to the inversion of an ill-conditioned matrix. Next, we present a first-order approximation of the noise term  $\mathbf{E}_L$  with respect to the additive perturbation in (25), using  $\mathbf{W}_0$  and  $\mathbf{W}_1$  to represent the noise-related Hankel matrices formed by the additive noise  $w(n)$ .

**Proposition 2.** Under Assumption 1, the  $i$ -th column of  $\mathbf{E}_L \in \mathbb{C}^{(N-L) \times M}$  defined in Proposition 1 is approximated by:

$$\mathbf{E}_L^i \cong \sum_{\substack{m=1 \\ m \neq i}}^M \frac{\mathbf{p}_m^H (\mathbf{W}_1 - z_i \mathbf{W}_0) \mathbf{q}_i}{b_i (\tilde{z}_i - z_m)} \begin{bmatrix} 1 \\ z_m \\ \vdots \\ z_m^{N-L-1} \end{bmatrix} + \frac{\mathbf{W}_0 \mathbf{q}_i}{b_i}, \quad (26)$$

provided that

$$\rho(\mathbf{D}_i \mathbf{T}_L^H \delta(\mathbf{X}_0^\dagger \mathbf{X}_1) \mathbf{T}_R) < 1, \quad (27)$$

where  $\rho(\mathbf{A})$  is the spectral radius of the matrix  $\mathbf{A}$ , and the matrix  $\mathbf{D}_i$  is an  $L \times L$  diagonal matrix defined by:

$$\mathbf{D}_i = \text{diag} \left( \frac{1}{\mathbf{p}_1^H \mathbf{q}'_1 (\tilde{z}_i - \lambda_1)}, \dots, 0_i, \dots, \frac{1}{\mathbf{p}_L^H \mathbf{q}'_L (\tilde{z}_i - \lambda_L)} \right). \quad (28)$$

*Proof.* See Appendix C in the SM.  $\square$

It is noteworthy that the condition in (27) and (28) implies a delicate balance between the  $i$ -th pole separation and perturbation (for details, see Remark 6 in Appendix C). In addition, note that the first term in the right hand side (r.h.s.) of (26) vanishes if  $\mathbf{W}_1 = z_i \mathbf{W}_0$ , i.e., when the noise signal  $w(n)$

consists only of the signal pole  $z_i$ . In such a degenerate case, the noise coincides with one of the signal's poles. Finally, we remark that Proposition 2 does not imply that the noise term  $\mathbf{E}_L$  is small. However, in the sequel, we show that the structure of  $\mathbf{E}_L$  in (26) allows us to extract and exploit the obscured Vandermonde structure of the signal modes in  $\tilde{\mathbf{Z}}_L$ .

Using Propositions 1 and 2, any signal mode  $\tilde{\mathbf{Z}}_L^i$ , can be expressed as:

$$\tilde{\mathbf{Z}}_L^i = \mathbf{Z}_L^i + \mathbf{E}_L^i, \quad 1 \leq i \leq M, \quad (29)$$

where  $\tilde{\mathbf{Z}}_L^i$ ,  $\mathbf{Z}_L^i$  and  $\mathbf{E}_L^i$  are the  $i$ -th columns of  $\tilde{\mathbf{Z}}_L$ ,  $\mathbf{Z}_L$  and  $\mathbf{E}_L$ , respectively.

Let  $\mathbf{Q}_i \in \mathbb{C}^{(N-L+1) \times N}$  be a convolution matrix, constructed from the vector  $\mathbf{q}_i \in \mathbb{C}^{L \times 1}$ , such that  $\mathbf{Q}_i \mathbf{v} = \mathbf{q}_i * \mathbf{v}$  and  $\mathbf{u}^T \mathbf{Q}_i = \mathbf{u}^T * \mathbf{q}_i$ , for any two vectors  $\mathbf{v} \in \mathbb{C}^{N \times 1}$  and  $\mathbf{u} \in \mathbb{C}^{(N-L+1) \times 1}$ . Combining this notation with (29) and Proposition 2, we have the following result.

**Corollary 1.** Any signal mode  $\tilde{\mathbf{Z}}_L^i$  can be recast as:

$$\tilde{\mathbf{Z}}_L^i \cong \begin{bmatrix} 1 \\ z_i \\ \vdots \\ z_i^{N-L-1} \end{bmatrix} + \sum_{\substack{m=1 \\ m \neq i}}^M \gamma_{i,m} \begin{bmatrix} 1 \\ z_m \\ \vdots \\ z_m^{N-L-1} \end{bmatrix} + \boldsymbol{\xi}_i, \quad (30)$$

where

$$\gamma_{i,m} = \frac{\mathbf{u}_m^T \mathbf{Q}_i \mathbf{w}}{(\tilde{z}_i - z_m) b_i}, \quad \boldsymbol{\xi}_i = \frac{\mathbf{I}_0 \mathbf{Q}_i \mathbf{w}}{b_i}, \quad (31)$$

the matrix  $\mathbf{I}_0$  is given by:

$$\mathbf{I}_0 = [\mathbf{I}_{N-L}, \mathbf{0}]_{(N-L) \times (N-L+1)},$$

where  $\mathbf{I}_{N-L}$  is the identity matrix of size  $N - L$  and  $\mathbf{0} \in \mathbb{C}^{(N-L) \times 1}$  is the zero vector. The vector  $\mathbf{u}_m \in \mathbb{C}^{(N-L+1)}$  is defined by:

$$\mathbf{u}_m^T = [0, \mathbf{p}_m^H] - z_i [\mathbf{p}_m^H, 0], \quad (32)$$

and  $\mathbf{w} = [w(0), \dots, w(N-1)]^T$  is the discrete noise vector introduced in (1) with  $\mathbb{E}[\mathbf{w} \mathbf{w}^H] = \sigma_w^2 \mathbf{I}_N$ .

Equation (30) shows that the signal modes consist of the true mode  $\mathbf{Z}_L^i$ , corrupted by two factors: (i) superimposed  $M - 1$  modes  $\mathbf{Z}_L^m$ ,  $m \neq i$  weighted by the coefficients  $\gamma_{i,m}$ , and (ii) a noise term  $\boldsymbol{\xi}_i$ . In the next result, we show that these two factors are controlled by the separation of the signal poles and the SNR at the  $i$ -th component, defined by:

$$\text{SNR}_i = \frac{|b_i|^2}{\sigma_w^2},$$

and in dB units as  $\text{SNR}_{i,\text{dB}} = 10 \log_{10}(\text{SNR}_i)$ .

**Proposition 3.** Under the conditions of Proposition 2, for any  $\varepsilon \in (0, 1)$ , the noise-related terms in (30) are bounded by:

$$|\gamma_{i,m}| \leq 2 \sqrt{\frac{2 \log(\frac{1}{\varepsilon})}{\text{SNR}_i}} \frac{\|\mathbf{u}_m * \mathbf{q}_i\|_2}{|z_i - z_m|}, \quad (33)$$

$$\|\boldsymbol{\xi}_i\|_\infty \leq \sqrt{\frac{2 \log(\frac{1}{\varepsilon})}{\text{SNR}_i}}, \quad (34)$$

with a probability of at least  $1 - \varepsilon$ , provided that:

$$|z_i - z_m| \geq 2|\delta z_i|, \quad 1 \leq m \neq i \leq M. \quad (35)$$

*Proof.* See Appendix D in the SM.  $\square$

Note that by (32),  $\mathbf{u}_m$  consists of the vector  $\mathbf{p}_m$ . Hence, the convolution  $\|\mathbf{u}_m * \mathbf{q}_i\|_2$  in (33) implicitly depends on the poles and the distances between the poles, as the vectors  $\mathbf{p}_m^H$  and  $\mathbf{q}_i$  are given by the  $m$ -th row of  $\mathbf{Z}_L^\dagger$  and  $i$ -th column of  $\mathbf{Z}_R^\dagger$ , respectively. Additionally, we remark that the condition in (35) is common in perturbation analysis. Informally, this condition guarantees that the signal poles  $z_i$  are sufficiently distinct relative to their perturbations.

Proposition 3 implies that the coefficients of the corrupting factors in (30) can be bounded with high probability by a function of the  $\text{SNR}_i$  and the  $i$ -th pole separation, provided that the separation is sufficiently large. This allows us to present the following signal mode detection method, which uses Fourier analysis, where the elements of the signal mode are viewed as a sequence consisting of a single tone corrupted by noise.

#### IV. STRUCTURE-AWARE MODEL ORDER DETECTION

In this section, we propose a detection method by identifying the signal modes. Based on Corollary 1, identifying the signal modes could be viewed as a relaxation of the original problem presented in (1) and (2); we are only interested in a *binary* detection, i.e., to determine whether the  $i$ -th mode is a signal mode or not, without parameter estimation. In turn, once the signal modes are identified, their corresponding eigenvalues enable us to estimate the signal parameters. By relying on the modes for the detection, this approach fundamentally differs from existing approaches, where only the singular values are considered for the model order detection. Specifically, we propose to detect the signal modes by applying the Discrete Fourier Transform (DFT) to the noisy modes<sup>2</sup>.

According to (30), the  $i$ -th signal mode is a composition of (i) a single tone (the  $i$ -th pole  $z_i$ ), (ii)  $M - 1$  attenuated tones (the other  $M - 1$  poles  $\{z_m\}_{m \neq i}$ ), and (iii) a noise component. To exploit this structure, we examine the DFT of  $\tilde{\mathbf{Z}}_L^i$  at the  $k$ -th frequency bin:

$$\mathcal{F}(\tilde{\mathbf{Z}}_L^i)[k] = \mathcal{D}(\theta_{i,k}) + \sum_{\substack{m=1 \\ m \neq i}}^M \gamma_{i,m} \mathcal{D}(\theta_{m,k}) + \mathcal{F}(\boldsymbol{\xi}_i)[k] \quad (36)$$

where  $1 \leq k \leq N - L$ ,  $\theta_{m,k} = \theta_m - \frac{2\pi k}{N-L}$  are modulated frequencies, and  $\mathcal{D}(\theta) = \frac{\sin(0.5\theta(N-L))}{\sin(0.5\theta)} e^{-j0.5\theta_{m,k}(N-L-1)}$  is the Dirichlet kernel of order  $N - L$ <sup>3</sup>.

The real-valued single-mode spectrum  $|\mathcal{F}(\tilde{\mathbf{Z}}_L^i)[k]|$  is examined, and since the maximum value of  $|\mathcal{D}(\theta)|$  is  $N - L$ ,  $|\mathcal{D}(\theta_{i,k})|$  is the dominant term of the spectrum in (36) if:

$$|\gamma_{i,m}| \ll \frac{1}{M-1}, \quad |\mathcal{F}(\boldsymbol{\xi}_i)[k]| \ll N - L. \quad (37)$$

<sup>2</sup>For the simplicity of the exposition, the derivation and analysis are presented under the assumption that the signal is undamped. In Section VII, we show that the proposed method performs well for damped signals as well.

<sup>3</sup>For simplicity, we ignore the DC component, assuming that the sum of elements of  $\tilde{\mathbf{Z}}_L^i$  equals 0, for  $1 \leq i \leq L$ ; in practice, we simply center each left mode by subtracting its mean.

In such cases,  $|\mathcal{F}(\tilde{\mathbf{Z}}_L^i)|$  exhibits a single dominant peak resulting from the term  $\mathcal{D}(\theta_{i,k})$ .

In the next result, we present an explicit condition on the problem parameters for which the conditions on the noise coefficient in (37) are met with high probability.

**Proposition 4.** For any  $\varepsilon \in (0, 1)$ , if the  $\text{SNR}_i$  is sufficiently high:

$$\frac{2\log(\frac{1}{\varepsilon})}{N-L} \ll \text{SNR}_i, \quad (38)$$

then the condition:

$$|\mathcal{F}(\boldsymbol{\xi}_i)[k]| \ll N - L,$$

is met with probability of at least  $1 - \varepsilon$ .

*Proof.* See Appendix E in the SM.  $\square$

Similarly, an explicit condition on  $\gamma_{i,m}$  is provided in the next proposition.

**Proposition 5.** For any  $\varepsilon \in (0, 1)$ , if the  $\text{SNR}_i$  is sufficiently high:

$$8\log(\frac{1}{\varepsilon})(M-1)^2 \frac{\|\mathbf{u}_m * \mathbf{q}_i\|_2^2}{|z_i - z_m|^2} \ll \text{SNR}_i, \quad (39)$$

then the condition:

$$|\gamma_{i,m}| \ll \frac{1}{M-1},$$

is met with probability of at least  $1 - \varepsilon$ , provided that:

$$|z_i - z_m| \geq 2|\delta z_i|, \quad \text{for } 1 \leq m \neq i \leq M.$$

*Proof.* Follows immediately by plugging (33) into (37).  $\square$

We note that in the case of two undamped signal poles, the terms  $\|\mathbf{u}_2 * \mathbf{q}_1\|_2$  and  $\|\mathbf{u}_1 * \mathbf{q}_2\|_2$  in (39) are two superimposed Dirichlet kernels, evaluated at  $\theta_2 - \theta_1$  and  $\theta_1 - \theta_2$ . Furthermore, numerical evaluation shows that, for a fixed  $N$ :

$$\|\mathbf{u}_1 * \mathbf{q}_2\|_2, \|\mathbf{u}_2 * \mathbf{q}_1\|_2 \propto \frac{1}{|\theta_1 - \theta_2|^2}, \quad (40)$$

illustrating that the term  $\|\mathbf{u}_m * \mathbf{q}_i\|_2$  in (39) is inversely proportional to the frequency separation in this simple case.

**Example 1.** To illustrate that conditions (38) and (39) in Propositions 4 and 5 are realistic, we simulate the signal (1) with two undamped exponentials,  $N = 101$ ,  $\alpha_1 = \alpha_2 = 0$ ,  $b_1 = b_2 = 1$ , and  $|\theta_2 - \theta_1| = \frac{1.5\pi}{N}$ . We set  $\varepsilon = 0.05$ , which results in:

$$\frac{2\log(\frac{1}{\varepsilon})}{N-L} \approx 0.09, \quad 8\log(\frac{1}{\varepsilon})(K-1)^2 \frac{\|\mathbf{u}_m * \mathbf{q}_i\|_2^2}{|z_i - z_m|^2} \approx 3.17.$$

We get that if  $5 \text{ dB} \ll \text{SNR}_{i,\text{dB}}$  then  $|\mathcal{F}(\boldsymbol{\xi}_1)[k]| \ll N - L$ , and  $|\gamma_{1,2}| \ll 1$  with a probability of at least 0.95.

**Remark 2.** We argue that the condition on  $\gamma_{i,m}$  can often be relaxed. First, we further observe that for close frequencies  $\theta_i$  and  $\theta_m$  such that  $|\theta_i - \theta_m| \leq \frac{2\pi}{N-L}$ , the kernels  $\mathcal{D}(\theta_{i,k})$  and  $\mathcal{D}(\theta_{m,k})$  in (36) are indistinguishable and form a single dominant peak. Hence, we only need to consider frequencies  $\theta_m$  that satisfy  $|\theta_i - \theta_m| > \frac{2\pi}{N-L}$ , so that the condition on  $|\gamma_{i,m}|$  in (37) is relaxed to  $|\gamma_{i,m}| \ll \frac{1}{K_i-1}$ ,

where  $K_i = \sum_{\substack{m=1 \\ m \neq i}}^M \mathbb{1}_{|\theta_i - \theta_m| > \frac{2\pi}{N-L}}$  is the number of frequencies  $\theta_m$  which are far enough from  $\theta_i$ , and  $\mathbb{1}_{|\theta_i - \theta_m| > \frac{2\pi}{N-L}}$  is an indicator function that equals 1 if  $|\theta_i - \theta_m| > \frac{2\pi}{N-L}$ , and 0 otherwise. We note that even after this relaxation, the required condition on  $\gamma_{i,m}$  is stringent. It refers to the worst-case where all the  $K_i$  frequencies  $\theta_{m,k}$  are far from  $\theta_{i,k}$  and do not fall within the main lobe of the Dirichlet kernel centered at  $\theta_{i,k}$ . Simultaneously, all these frequencies  $\theta_{m,k}$  are closely-spaced and the main lobes of their Dirichlet kernels overlap. Therefore, further relaxation of this condition could be  $|\gamma_{i,m}| \ll \frac{1}{K_i}$ , assuming the existence of a cluster of at most  $K'_i \ll K_i$  closely-spaced frequencies.

In summary, if the  $i$ -th mode  $\tilde{\mathbf{Z}}_L^i$  is a signal mode, we expect, by Propositions 4 and 5, a single dominant peak in  $|\mathcal{F}(\tilde{\mathbf{Z}}_L^i)|$ , when a certain balance between the SNR $_i$ , the modes dimension  $N - L$ , and the  $i$ -th pole separation is maintained. This balance was shown to be realistic in Example 1. In contrast, if the  $i$ -th mode is not a signal mode, it does not have any specific structure, and therefore, we expect an arbitrary DFT spectrum, different than the signal-modes spectrum. See illustration in Fig. 2. Next, we leverage this distinction to design detection features for identifying the signal modes, which are also employed as an order detection rule.

#### A. Signal mode detection features

We propose a simple feature to decide whether a single-mode spectrum is associated with a signal or noise. We suggest computing the maximum value of the single-mode spectrum  $|\mathcal{F}(\tilde{\mathbf{Z}}_L^i)[k]|$  for the  $i$ -th mode. That is, we compute:

$$\epsilon_i = \max_{1 \leq k \leq N-L} |\mathcal{F}(\tilde{\mathbf{Z}}_L^i)[k]|, \quad 1 \leq i \leq L, \quad (41)$$

Intuitively, large values of  $\epsilon_i$  indicate that  $\tilde{\mathbf{Z}}_L^i$  is a signal mode. Conversely, as noise modes lack a particular structure, small values of  $\epsilon_i$  indicate that  $\tilde{\mathbf{Z}}_L^i$  is a spurious noise mode. In the sequel, we describe how to leverage this intuition to design a systematic detection.

An additional advantage of determining the model order from the modes, rather than the singular values, is the ability to use additional information about the frequencies associated with each mode, which can be used to refine the features in (41). If two frequencies  $\theta_1$  and  $\theta_2$  are separated by less than  $\frac{4\pi}{N}$ , their corresponding Dirichlet kernels will overlap, resulting in an increased value in their single-mode spectrum. Therefore, when clusters of closely-spaced frequencies are present, their Dirichlet kernels will overlap significantly, causing an even greater increase in their single-mode spectrum. This effect amplifies the peaks in the spectrum, making the clusters of close frequencies more pronounced compared to isolated frequencies. Consequently, we suggest a normalized version of (41) that can be interpreted as a sharpness ratio:

$$\epsilon_i = \frac{1}{d_{\theta_i}} \max_{1 \leq k \leq N-L} |\mathcal{F}(\tilde{\mathbf{Z}}_L^i)[k]|, \quad (42)$$

where

$$d_{\theta_i} = \sum_{m=1}^L |\hat{\theta}_i - \hat{\theta}_m|^2,$$

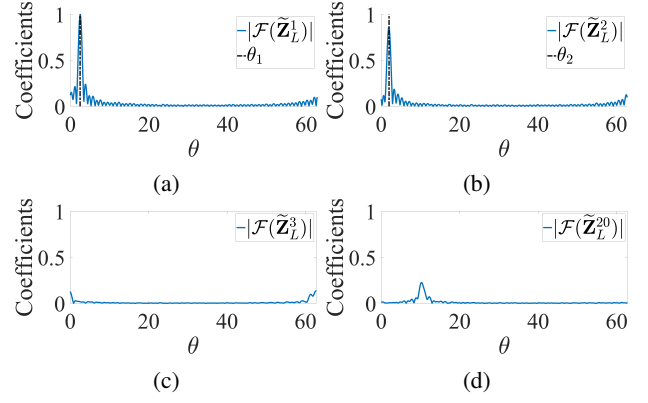


Fig. 2: Normalized DFT coefficients of four different modes are shown. The first and second signal modes are displayed in (a) and (b), while two randomly selected noise modes are shown in (c) and (d). The simulated signal consists of two undamped exponentials, with  $N = 101$ ,  $\alpha_1 = \alpha_2 = 0$ ,  $b_1 = b_2 = 1$ , and  $|\theta_2 - \theta_1| = \frac{1.5\pi}{N}$ . The SNR $_{dB}$  is set to 10 dB.

is a measure of the frequencies spread around the spectrum peak, and the frequencies  $\{\hat{\theta}_m\}_{m=1}^L$ , are extracted from the corresponding poles, according to (12).

The set of features  $\{\epsilon_i\}_{i=1}^L$  in (41) or (42) can be used to determine the model order by dividing them into two distinct subsets: signal-related and noise-related. The cardinality of the signal-related subset then determines the model order. The proposed normalized features in (42) render the signal-related features in (41) more homogeneous, making them well-suited for binary clustering. Therefore, we propose to use the k-means algorithm with  $k = 2$ , for this division. In Sec. VI we incorporate this order detection step in the proposed SAMP algorithm.

**Remark 3.** We do not use the DFT here for frequency estimation, but only for signal mode detection. The frequency estimation is implemented using the eigenvalues corresponding to the identified signal modes. In contrast to the DFT, these eigenvalues are not restricted to a regular grid that limits the resolution. Additionally, the corrupting term  $\sum_{\substack{m=1 \\ m \neq i}}^M \gamma_{i,m} \mathcal{D}(\theta_{m,k})$ , might cause a bias in the dominant frequency of  $\mathcal{F}(\tilde{\mathbf{Z}}_L^i)$ .

**Remark 4.** We leveraged the Vandermonde structure globally, by examining the DFT of the modes. Alternatively, we could follow a local perspective, viewing each signal mode in (30) as a column of a perturbed Vandermonde matrix, demonstrating a near multiplicative structure. For example, in the context of DMD, Bronstein et al. [43] introduced a detection feature based on the mean ratio of consecutive rows of the DMD modes (see Appendix F in the SM for more details). Our simulations show that using the global features in (42) is superior to such 'local' approaches, both in accuracy and computational complexity, and therefore, their empirical results are not presented in the sequel.

## V. EFFICIENT AMPLITUDES EXTRACTION

We propose a computationally efficient approach for estimating the amplitudes, leveraging the structure of the MP modes as described in Proposition 1 and more generally in Theorem 1, Appendix B. In these results, we show that the first row of  $\tilde{\mathbf{Z}}_L$  is given by:

$$\mathbf{e}_1^T \tilde{\mathbf{Z}}_L = \left[ [\sqrt{b_1}, \dots, \sqrt{b_M}] + \mathbf{e}_1^T \mathbf{E}_L \sqrt{\mathbf{B}}, \mathbf{e}_1^T \mathbf{C}_L \right] \in \mathbb{C}^{1 \times L},$$

and similarly, the first column of  $\tilde{\mathbf{Z}}_R$  is given by:

$$\tilde{\mathbf{Z}}_R \mathbf{e}_1 = \left[ [\sqrt{b_1}, \dots, \sqrt{b_M}]^T + \sqrt{\mathbf{B}} \mathbf{E}_R \mathbf{e}_1 \right] \in \mathbb{C}^{L \times 1}$$

where the vector  $\mathbf{e}_1$  is the standard unit vector, and the matrices  $\mathbf{C}_L \in \mathbb{C}^{(N-L) \times (L-M)}$ , and  $\mathbf{C}_R \in \mathbb{C}^{(L-M) \times L}$  are  $L-M$  noise-related spurious columns and rows, respectively. Consequently, we propose to estimate the amplitudes by the following element-wise multiplication:

$$\hat{\mathbf{b}} = (\mathbf{e}_1^T \tilde{\mathbf{Z}}_L)^T \odot (\tilde{\mathbf{Z}}_R \mathbf{e}_1) \in \mathbb{C}^L, \quad (43)$$

where  $\hat{\mathbf{b}}$  consists of the estimated amplitudes, and the  $i$ -th entry of  $\hat{\mathbf{b}}$  is given by:

$$\hat{b}_i = \begin{cases} b_i(1 + \mathbf{E}_L(1, i))(1 + \mathbf{E}_R(i, 1)) & , \text{if } 1 \leq i \leq M, \\ \mathbf{C}_L(1, i - M) \mathbf{C}_R(i - M, 1) & , \text{if } M < i \leq L \end{cases}$$

This method involves simple element-wise multiplication of two vectors in  $\mathbb{C}^L$ , requiring  $\mathcal{O}(L)$  operations. The existing method in (14) involves pseudo-inverting a matrix of size  $N \times \hat{M}$ , where  $\hat{M}$  is based on the truncated-SVD of  $\mathbf{Y}_0$ , and hence  $1 \leq \hat{M} \leq L < N$ . The computational complexity of the existing method is  $\mathcal{O}(N\hat{M}^2 + \hat{M}^3)$ . As noted in Section II, estimating the model order using the truncated-SVD step is prone to over- or underestimation. In the extreme case of underestimation, where  $\hat{M} = 1$ , the existing method requires  $\mathcal{O}(N)$  operations, while if  $\hat{M} = L$ , the existing method requires  $\mathcal{O}(NL^2 + L^3)$  operations. Either way, the proposed approach is more efficient. In Section VII, we compare its performances to the existing method for estimating the signal amplitudes given in (14), which is based on matrix inversion.

We highlight that similarly to Sec. IV, where spectral information is extracted from the MP modes to identify signal-related components, in (43), temporal information is extracted from the MP modes to estimate the noisy amplitudes efficiently. This new approach of extracting meaningful information from the MP modes fundamentally differs from existing approaches, where the MP modes (or eigenvectors) are not typically recognized as carrying valuable information for estimating the signal parameters.

## VI. PROPOSED ALGORITHM

Relying on the analysis and results regarding model order detection and amplitude estimation in Sections IV and V, we present the Structure-Aware Matrix Pencil (SAMP) algorithm, which is summarized in Algorithm 1. Compared to the standard MP method, our main novelties are the detection of signal modes, a new model order detection approach, and efficient amplitude estimation.

## A. Practical Considerations

Although the proposed model order detection method does not require truncation in (4), our numerical studies indicate that removing strong noise-related components can reduce the bias of the estimates. Therefore, we recommend using a weak-truncation method in (4) to eliminate strong noise components only. By our simulations, an example of such a method is the effective rank, introduced in [44]. The effective rank method estimates the dimensionality or rank of a matrix in the presence of noise by utilizing the entropy of its normalized singular values. Given a set of singular values  $\{\sigma_i\}_{i=1}^L$ , the normalized singular values are defined as  $p_i = \frac{\sigma_i}{\sum_{j=1}^L \sigma_j}$ . The entropy  $H(\mathbf{p})$  of these normalized singular values is calculated using  $H(\mathbf{p}) = -\sum_{i=1}^n p_i \log(p_i)$ , and the effective rank is then defined as  $\exp(H(\mathbf{p}))$ . The model order is estimated by:

$$\widehat{M}_{\text{ER}} = \text{round}(\exp(H(\mathbf{p}))). \quad (44)$$

**Remark 5.** *The proposed SAMP algorithm (Algorithm 1) deviates from the conventional “detect and then estimate” strategy. Instead, it adopts an “estimate and then select” approach, wherein the model parameters are first estimated from the eigenvalues and modes, and then, the signal-related components are detected based on these estimated parameters.*

## B. Computational complexity

We evaluate the computational complexity of the proposed algorithm by counting the number of complex operations required for each step. In step 1, we compute the modes and eigenvalues. This step requires  $\mathcal{O}((N-L)L^3)$  operations. In step 2, we estimate the signal parameters. This step requires  $\mathcal{O}(L)$  operations. In step 3, we determine the model order. First we compute the  $L$  measures  $\{\epsilon_i\}_{i=1}^L$  using (42), which requires  $\mathcal{O}(L(N-L)\log(N-L))$  operations. Next, we divide the set  $\{\epsilon_i\}_{i=1}^L$  into two distinct subsets, which typically requires  $\mathcal{O}(L)$  operations. In step 4, we select the signal-related parameters. This step requires  $\mathcal{O}(\widehat{M})$  operations. The overall complexity of the proposed algorithm is  $\mathcal{O}((N-L)L^3)$ . For comparison, the overall complexity of the standard MP algorithm is also  $\mathcal{O}((N-L)L^3)$ , and the most demanding step in both methods is the calculation of the matrix  $\mathbf{A}$  which involves the multiplication of four matrices.

## VII. NUMERICAL RESULTS

In this section, we present simulation results focusing on two closely-spaced frequencies at low SNR values. We begin by showcasing the detection and estimation capabilities of the proposed SAMP algorithm (Algorithm 1). Then, we focus on the proposed amplitude estimation method and compare it in terms of computation time and accuracy to the traditional amplitude estimation method in (14).

We compare the proposed SAMP algorithm with five other methods based on singular value truncation. Two of these methods use the *coupled detection and estimation* approach. Specifically, we consider the MDL and AIC criteria (see Sec. II-A for details). We emphasize that these methods rely on computing the likelihood function, which requires prior

---

**Algorithm 1** SAMP proposed algorithm
 

---

**Input:** Noisy measurement  $\{y(n)\}_{n=1}^N$ , pencil parameter  $L$ .

**Output:** Estimates of the signal frequencies, damping factors, and amplitudes.

1: Modes and Eigenvalues Computation:

- Construct the Hankel matrices  $\mathbf{Y}_0, \mathbf{Y}_1$  from the measured signal  $\{y(n)\}_{n=0}^{N-1}$  by (3).
- Compute the truncated-SVD of  $\mathbf{Y}_0 \approx \mathbf{U}\Sigma\mathbf{V}^H$ , using the effective-rank method by (44).
- Decompose the matrix  $\mathbf{A} = \Sigma^{-1}\mathbf{U}^H\mathbf{Y}_1\mathbf{V}$  to get  $\mathbf{A}\mathbf{Q} = \mathbf{Q}\hat{\mathbf{A}}$ , by (7).
- Calculate the left MP modes  $\tilde{\mathbf{Z}}_L = \mathbf{U}\Sigma\mathbf{Q}$  by (20).

2: Parameter Estimation:

- Estimate the frequencies and damping factors by (12):

$$\hat{\theta}_i = \arg(\tilde{\lambda}_i), \quad \hat{\alpha}_i = \log|\tilde{\lambda}_i|, \quad 1 \leq i \leq L.$$

- Estimate the complex amplitudes by (43):

$$\hat{\mathbf{b}} = (\mathbf{e}_1^T \tilde{\mathbf{Z}}_L)^T \odot (\tilde{\mathbf{Z}}_R \mathbf{e}_1).$$

3: Model Order Detection:

- Compute the  $L$  features by (42):

$$\epsilon_i = \frac{1}{d_{\theta_i}} \max_{1 \leq k \leq N-L} |\mathcal{F}(\tilde{\mathbf{Z}}_L^i)[k]|, \quad 1 \leq i \leq L.$$

- Partition the set  $\{\epsilon_i\}_{i=1}^L$  into two distinct subsets and select the subset with the largest average value.
- Set the model order to:  $\hat{M} = |\mathcal{S}|$ , where  $\mathcal{S}$  is the set of indices corresponding to the subset with the largest average value.

4: Parameter Selection:

- Select the signal components by:  $\hat{\theta}_s, \hat{\alpha}_s, \hat{b}_s, \quad s \in \mathcal{S}$ .
- 

knowledge of the noise distribution (which is unknown in our setting) and is computationally inefficient since the likelihood must be calculated for every possible hypothesized model order. The remaining methods use the *decoupled detection and estimation* approach, which is the standard practice in the MP literature. In particular, we examine the Significant Decimal Digits (SDD) method with  $p = 2$  and  $p = 3$  (see Section II-A), a widely used method in the MP literature [29]–[31], [38], [39]. Additionally, we evaluate the GAP method, introduced in Sec. II-A, which is another common approach for SVD truncation [33], [40]. For a fair comparison, we also include the effective rank method (EFF) [44], as we use it in our algorithm to eliminate strong noise-related components in the SV truncation step. In our simulations, the SDD method yielded significantly lower performance than the GAP and EFF methods, and we omitted its results.

Throughout this section, we simulate a sum of two complex exponentials with closely-spaced frequencies, given by (2) with  $M = 2$ ,  $b_1 = b_2 = 1$ , and  $\phi_1 = \phi_2 = 0$ . Additionally, we set  $L = \text{round}(N/3)$ . We conduct two experiments. In the first experiment, we consider a sum of two *undamped* exponentials by setting  $\alpha_1 = \alpha_2 = 0$  in (2), while in the second experiment, we consider a sum of two *damped* exponentials by setting

$\alpha_1 = 0.03$ , and  $\alpha_2 = 0.05$  in (2). Our goal is twofold. Given a finite sample of the noisy signal  $y(n)$ , as in (1), we aim to detect the model order (the number of complex exponentials), which is 2 in our simulations, and estimate the corresponding two frequencies and damping factors. The code to reproduce all the results in this section is available in the following GitHub link.

#### A. Model order detection

We determine the probability of correctly identifying the model order,  $p_d$ , defined by:

$$p_d = \mathbb{P}(\hat{M} = M) \cong \frac{1}{N_{\text{exp}}} \sum_{i=1}^{N_{\text{exp}}} \mathbb{1}_{\hat{M}=M},$$

where  $N_{\text{exp}} = 500$  is the number of independent Monte-Carlo trials, and  $\mathbb{1}_{\hat{M}=M}$  is an indicator function that equals 1 if the estimated model order  $\hat{M}$  matches the true model order  $M$ , and 0 otherwise. We also present the Area Under the Curve (AUC) for each method to simplify the comparisons between the methods.

Figs. 3a-3b display  $p_d$  versus the SNR in dB, for  $N = 101$  samples,  $\theta_1 = 2$  rad/sample, and  $\theta_2 = \theta_1 + \frac{1.5\pi}{N}$ . The value of  $\theta_2$  is set because the difference  $|\theta_2 - \theta_1| = \frac{1.5\pi}{N}$  is smaller than the Rayleigh limit [45]. The SNR is defined as:

$$\text{SNR} = \sum_{i=1}^M \frac{|b_i|^2}{\sigma_w^2},$$

and we denote  $\text{SNR}_{\text{dB}} = 10\log_{10}(\text{SNR})$ . Fig. 3c-3d display  $p_d$  versus the number of samples  $N$ , for  $\text{SNR}_{\text{dB}}$  value of 10 dB,  $\theta_1 = 2$  rad/sample, and  $\theta_2 = \theta_1 + \frac{1.5\pi}{N}$ . Fig. 3e-3f display  $p_d$  versus the distance between frequencies  $|\Delta\theta|$ , for  $\text{SNR}_{\text{dB}}$  value of 10 dB, and  $N = 101$  samples.

We see that the proposed SAMP method outperforms the GAP and EFF methods by a large margin in all the presented scenarios. Specifically, it is worth noting that the EFF method fails as a stand-alone detection method, but in the proposed SAMP approach, we use it as a pre-processing step to eliminate the strong noise components. Empirically, we see that the EFF consistently overestimates the model order, even for high  $\text{SNR}_{\text{dB}}$  values. Additionally, the SAMP method outperforms the MP-based AIC criterion and archives compatible results with the MP-based MDL criterion, even though it does not assume any prior knowledge about the noise distribution. We note that the GAP method can also be applied to the proposed detection features  $\{\epsilon_i\}_{i=1}^L$  from (42). Replacing the k-means algorithm in step 3 in the proposed algorithm with the GAP method, provides similar AUC results and is more computationally efficient.

*Robustness to noise distribution:* to highlight that the proposed SAMP method is distribution-free, unlike the MDL and AIC methods, we also simulate non-Gaussian additive noise. Table I shows the AUC of  $p_d$  versus the  $\text{SNR}_{\text{dB}}$  (in the range of 0-30 dB) for each method under different noise distributions. The first experiment (second column from left) depicts the results of a normal distribution, as seen in Figs. 3a-3b. In the

second experiment (third column from left), we simulated a Bi-normal distribution:

$$\mathcal{B}_d = \mathbb{1}_{p < r} \cdot \mathcal{N}(\mu_1, \sigma_1) + \mathbb{1}_{p \geq r} \cdot \mathcal{N}(\mu_2, \sigma_2),$$

where  $p$  is a random number drawn from the standard uniform distribution on the open interval  $(0, 1)$ , and  $r$  is a pre-defined threshold, set to  $r = 0.85$  in our simulations. In the third experiment (rightmost column), we simulated uniform distribution. The results demonstrate that the proposed SAMP method is robust to distribution shifts, and maintains a consistent AUC score across all distribution types. In contrast, the MDL and AIC methods exhibit high degradation.

### B. Parameter estimation

First, we present the distribution of the estimated parameter of interest for each method, as each method can underestimate or overestimate the true model order. Fig. 4 shows the estimated frequency distribution for each method in the undamped case, along with their estimated PDFs.

We see that the proposed SAMP method outperforms the standard *decoupled detection and estimation* methods, producing a ‘Gaussian-like’ distribution centered around the true frequencies, where the GAP and EFF methods fall short. Specifically, the EFF method systematically estimates more than two components, resulting in a relatively wide and diffuse frequency distribution, while the GAP method estimates only one component for moderate to low  $\text{SNR}_{\text{dB}}$  values, resulting in a biased ‘Gaussian-like’ distribution. The SAMP method and the MDL and AIC methods yield similar distributions. The complementary results of the damped case show similar trends and are presented in Appendix G, Fig. 8.

Next, we evaluate the empirical bias and the Root Mean Squared Error (RMSE) of an estimate  $\hat{\eta}$  of a parameter of interest  $\eta$  which are defined by:

$$\begin{aligned} \text{bias}(\hat{\eta}) &= \frac{1}{N_{\text{exp}}} \sum_{i=1}^{N_{\text{exp}}} \hat{\eta}_i - \eta \\ \text{RMSE}(\hat{\eta}) &= \frac{1}{N_{\text{exp}}} \sum_{i=1}^{N_{\text{exp}}} (\hat{\eta}_i - \eta)^2 \end{aligned}$$

where  $\{\hat{\eta}_i\}_{i=1}^{N_{\text{exp}}}$  is the estimate of  $\eta$  in the  $i$ -th Monte-Carlo trial, and  $N_{\text{exp}} = 500$  is the number of independent Monte-Carlo trials. If more than two components are detected, we evaluate the closest estimated parameter to the true parameter of interest.

Fig. 5 displays the  $\text{RMSE}(\hat{\theta}_1)$  in dB of the estimate  $\hat{\theta}_1$  versus the  $\text{SNR}_{\text{dB}}$ . The complementary figures of the empirical bias of the estimate  $\hat{\theta}_1$  are presented in Appendix G, Fig. 9. We include the Cramer-Rao lower bound (CRB) as a reference for evaluating the variance of  $\hat{\theta}_1$  (see [3], [4] for details). All the competing methods show nearly unbiased estimates for  $\text{SNR}_{\text{dB}}$  values above a certain threshold, as shown in Appendix G, Fig. 9. Therefore, following the approach presented in [33], we use the CRB for an unbiased estimator as a reference for the competing methods. For unbiased estimators, the RMSE simplifies to the square root of the variance, since

$\text{RMSE}^2(\hat{\theta}_1) = \text{var}(\hat{\theta}_1) + \text{bias}^2(\hat{\theta}_1)$ . We note that the GAP method is heavily biased and the presented CRB does not apply to it.

We see in Figs. 5a and 5b that the SAMP method has similar results to the MDL and AIC methods, nearly achieving the CRB, and outperforming the traditional GAP method for moderate to low  $\text{SNR}_{\text{dB}}$  values. We highlight again that the MDL and AIC methods assume that the noise distribution is known, while the proposed SAMP method is distribution-free, as evidenced by Table I. Seemingly, the EFF method achieves comparable results. However, this is a side-effect of evaluating the estimated frequency that is closest to the true frequency, in case of overestimating the model order. We note that for very low  $\text{SNR}_{\text{dB}}$  values, the GAP method performs better than the SAMP method. This is because the GAP method consistently detects only one component as a signal component in low  $\text{SNR}_{\text{dB}}$  values (see Figs. 3a-3b, and 4). Evidently, for closely-spaced frequencies and very low  $\text{SNR}_{\text{dB}}$  values, this approach achieves the best results.

To qualitatively evaluate the results, we depict half of the  $i$ -th frequency separation, defined by

$$\text{sep}(i) = \min_{\substack{m=1, \dots, M \\ m \neq i}} |\theta_i - \theta_m|,$$

for reference. In the case of two frequencies, the frequency separation is just  $|\theta_1 - \theta_2|$ . This value forms a reasonable threshold for the frequency estimation error

$$\text{RMSE}(\hat{\theta}_i) < \frac{\text{sep}(i)}{2}, \quad (45)$$

as it guarantees that the estimated frequencies are well separated from each other (theoretical frequency resolution limits are also discussed in [46], [47]). Indeed, we see in Fig. 5a that the  $\text{RMSE}(\hat{\theta}_1)$  of the SAMP method is lower than this threshold, depicted as the gray line in the figure, for almost the entire  $\text{SNR}_{\text{dB}}$  range. Note that the  $\text{RMSE}(\hat{\theta}_i)$  of the GAP method and  $\frac{\text{sep}(i)}{2}$  coincide. The reason is that the GAP method detects only one component (see Figs. 3a-3b, and 4c), which results in estimating the average frequency  $\frac{\theta_1 + \theta_2}{2}$  and not  $\theta_1$ . In such cases,  $\text{RMSE}(\hat{\theta}_i) = \frac{|\theta_1 - \theta_2|}{2}$ , which is exactly  $\frac{\text{sep}(i)}{2}$ . The complementary results of the  $\text{RMSE}(\hat{\theta}_1)$  in dB and the absolute value of the empirical bias of the estimate  $\hat{\theta}_1$  versus the number of samples, and the frequencies distance show similar trends and are presented in Appendix G, Fig. 10 and Fig. 11, respectively. Comparable results for  $\hat{\theta}_2$  (see for example Fig. 4) are omitted for brevity.

*Computational load:* to demonstrate the superior computational efficiency of the proposed SAMP method compared to the MDL and AIC methods, we present the frequency estimation error for each method as a function of the computation time for different signal lengths in Fig. 6. The error is defined as the sum of the RMSE between each true frequency and the closest two estimated frequencies. The figures show that the proposed SAMP method consistently achieves the same RMSE levels for the undamped case, and slightly higher RMSE levels for the damped case, compared to the MDL and AIC methods, but in significantly lower computation time.

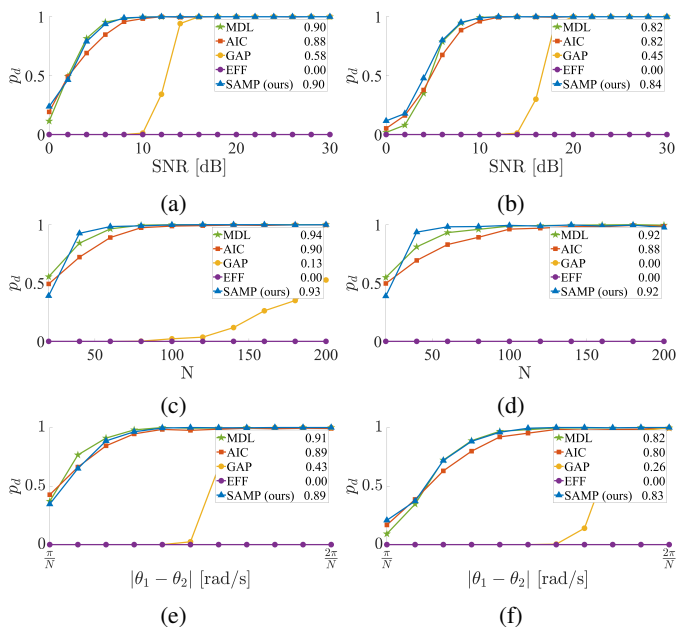


Fig. 3: Probability of correct model order estimation versus: (a)-(b)  $\text{SNR}_{\text{dB}}$ , (c)-(d) number of samples, and (e)-(f) frequency distance. Undamped case in the left column, damped case in the right column. AUC scores for each method are provided in the legend.

TABLE I: AUC Comparison of Different Methods under Various Noise Distributions, for the undamped (undmp), and damped (dmp) cases. The proposed SAMP method shows robustness to changes in noise distribution.

Method	Normal		Bi-normal		Uniform	
	undmp	dmp	undmp	dmp	undmp	dmp
MDL	<b>0.90</b>	0.82	0.82	0.75	0.34	0.37
AIC	0.88	0.82	0.78	0.72	0.31	0.34
GAP	0.58	0.45	0.55	0.43	0.33	0.38
EFF	0.00	0.00	0.00	0.00	0.00	0.00
SAMP (ours)	<b>0.90</b>	<b>0.84</b>	<b>0.90</b>	<b>0.85</b>	<b>0.91</b>	<b>0.85</b>

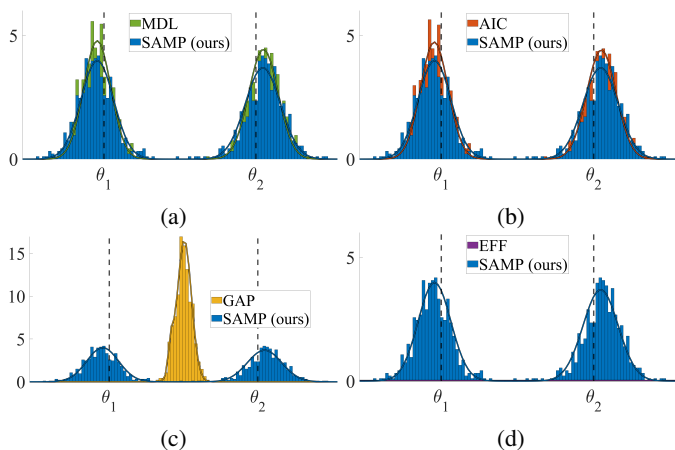


Fig. 4: Estimated frequencies distribution of all competing methods in the undamped case, at  $\text{SNR}_{\text{dB}}$  level of 10 dB.

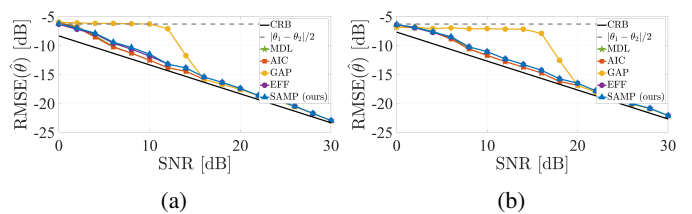


Fig. 5:  $\text{RMSE}(\hat{\theta}_1)$  versus the  $\text{SNR}_{\text{dB}}$ . Undamped case in (a), damped case in (b).

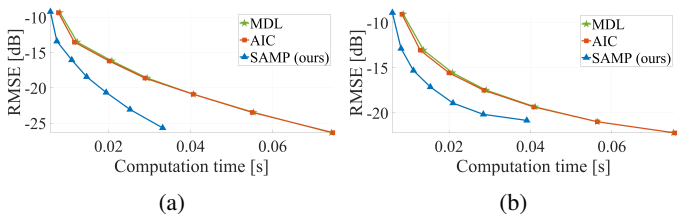


Fig. 6: Computational time comparison between the proposed SAMP, MDL, and AIC methods. Undamped case in (a), damped case in (b). The maximal SNR model order for the MDL and AIC methods is 10, and the  $\text{SNR}_{\text{dB}}$  level is 10 dB.

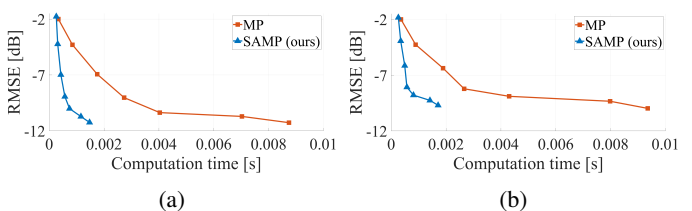


Fig. 7: Computational time comparison between the proposed amplitude estimation method, and the standard amplitude estimation method. Undamped case in (a), damped case in (b). In both cases  $|\theta_2 - \theta_1| = \frac{1.5\pi}{N}$ . The  $\text{SNR}_{\text{dB}}$  value is 10 dB.

### C. Amplitudes Estimation

In (43) in Section VI, we presented a computationally efficient approach for estimating the noisy amplitudes. We evaluate the performance of our method in comparison to the standard amplitude estimation technique presented in (14). We set  $r = L$  to concentrate only on the amplitude estimation, circumventing any possible overestimation or underestimation of the model order by any of the methods.

Fig. 7 displays the amplitude estimation error for each method as a function of the computation time for different signal lengths. The error is defined as the sum of the RMSE between each of the true amplitudes and the closest two estimated amplitudes. We see in the figure that the proposed method consistently obtains the same RMSE level as the standard method in considerably lower computation time.

## VIII. CONCLUSION

We addressed the problem of detecting the number of complex exponentials and estimating their parameters from noisy measurements using the MP method. We introduced the concept of MP modes,  $\hat{\mathbf{Z}}_L$ , through an extension of the MP

theorem to noisy conditions, revealing their informative structure. Specifically, we showed that the signal-related modes can be expressed as an obscured Vandermonde matrix,  $\mathbf{Z}_L + \mathbf{E}_L$ , and provided a detailed characterization of the noise-induced term  $\mathbf{E}_L$ . By leveraging the spectral structure of the signal-related modes and utilizing the noise-term characterization, we showed that temporal information can be effectively extracted, significantly improving model order selection, which often solely relies on singular values and thresholding heuristics. Utilizing the MP modes, we proposed the SAMP algorithm for detecting and estimating the signal-related components, along with a computationally efficient method for estimating the signal's amplitudes.

Our simulations indicate that the proposed method outperforms the classical thresholding-based competing methods by a large margin in detecting the model order, and nearly achieves the CRB for a broad SNR range, surpassing all other classical thresholding-based competitors, in estimating the signal's parameters. When compared to *coupled detection-estimation* approaches, such as MDL and AIC, the proposed method achieves comparable or better results with significantly lower computational time. Additionally, unlike MDL and AIC, the proposed method does not require prior knowledge of the noise distribution and was shown to be insensitive to various noise distributions.

We postulate that our approach is general, and it is not restricted to the MP method only. For example, several related methods generate Hankel matrices similar to the MP method and use a truncated SVD step to reduce noise. These include the SVD-based Prony method [48], State Space method (SSM) [49], Dynamic Mode Decomposition (DMD) [34], and Singular Spectrum Analysis (SSA) [50], [51]. In future research, we will extend these findings to multivariate signals and explore the concept of *modes* in other super-resolution methods, such as root-MUSIC [52] and ESPRIT [9].

#### REFERENCES

- [1] D. B. Percival and A. T. Walden, *Spectral analysis for physical applications*. Cambridge University Press, 1993.
- [2] S. M. Kay and S. L. Marple, "Spectrum analysis—a modern perspective," *Proc. IEEE*, vol. 69, no. 11, pp. 1380–1419, 1981.
- [3] P. Stoica, R. L. Moses, *et al.*, *Spectral analysis of signals*. Pearson Prentice Hall Upper Saddle River, NJ, 2005, vol. 452.
- [4] S. Lang and J. McClellan, "Frequency estimation with maximum entropy spectral estimators," *IEEE Trans. Acoust. Speech Signal Process.*, vol. 28, no. 6, pp. 716–724, 1980.
- [5] T. Abatzoglou, "A fast maximum likelihood algorithm for frequency estimation of a sinusoid based on Newton's method," *IEEE Trans. Acoust. Speech Signal Process.*, vol. 33, no. 1, pp. 77–89, 1985.
- [6] Y. Bresler and A. Macovski, "Exact maximum likelihood parameter estimation of superimposed exponential signals in noise," *IEEE Trans. Acoust. Speech Signal Process.*, vol. 34, no. 5, pp. 1081–1089, 1986.
- [7] J. Capon, "High-resolution frequency-wavenumber spectrum analysis," *Proc. IEEE*, vol. 57, no. 8, pp. 1408–1418, 1969.
- [8] R. Schmidt, "Multiple emitter location and signal parameter estimation," *IEEE Trans. Antennas Propag.*, vol. 34, no. 3, pp. 276–280, 1986.
- [9] R. Roy and T. Kailath, "Esprit-estimation of signal parameters via rotational invariance techniques," *IEEE Trans. Acoust. Speech Signal Process.*, vol. 37, no. 7, pp. 984–995, 1989.
- [10] P. Stoica and K. C. Sharman, "Maximum likelihood methods for direction-of-arrival estimation," *IEEE Trans. Acoust. Speech Signal Process.*, vol. 38, no. 7, pp. 1132–1143, 1990.
- [11] P. Stoica, P. Babu, and J. Li, "New method of sparse parameter estimation in separable models and its use for spectral analysis of irregularly sampled data," *IEEE Trans. Signal Process.*, vol. 59, no. 1, pp. 35–47, 2010.
- [12] L. Hu, Z. Shi, J. Zhou, and Q. Fu, "Compressed sensing of complex sinusoids: An approach based on dictionary refinement," *IEEE Trans. Signal Process.*, vol. 60, no. 7, pp. 3809–3822, 2012.
- [13] M. F. Duarte and R. G. Baraniuk, "Spectral compressive sensing," *Appl. Comput. Harmon. Anal.*, vol. 35, no. 1, pp. 111–129, 2013.
- [14] G. Tang, B. N. Bhaskar, P. Shah, and B. Recht, "Compressed sensing off the grid," *IEEE Trans. Inf. Theory*, vol. 59, no. 11, pp. 7465–7490, 2013.
- [15] L. Hu, J. Zhou, Z. Shi, and Q. Fu, "A fast and accurate reconstruction algorithm for compressed sensing of complex sinusoids," *IEEE Trans. Signal Process.*, vol. 61, no. 22, pp. 5744–5754, 2013.
- [16] Z. Yang, J. Li, P. Stoica, and L. Xie, "Sparse methods for direction-of-arrival estimation," in *Academic Press Library in Signal Process., Volume 7*, Elsevier, 2018, pp. 509–581.
- [17] Y. Chu, Z. Wei, and Z. Yang, "New reweighted atomic norm minimization approach for line spectral estimation," *Signal Process.*, vol. 206, p. 108 897, 2023.
- [18] X. Wu, Z. Yang, J.-F. Cai, and Z. Xu, "Spectral super-resolution on the unit circle via gradient descent," in *Int. Conf. on Acoust. Speech Signal Process. (ICASSP)*, IEEE, 2023, pp. 1–5.
- [19] F. Andersson, M. Carlsson, J.-Y. Tournier, and H. Wendt, "Frequency estimation based on Hankel matrices and the alternating direction method of multipliers," in *21st European Signal Process. Conf. (EUSIPCO 2013)*, IEEE, 2013, pp. 1–5.
- [20] B. Hayes, C. Saitis, and G. Fazekas, "Sinusoidal frequency estimation by gradient descent," in *Int. Conf. on Acoust. Speech Signal Process. (ICASSP)*, IEEE, 2023, pp. 1–5.
- [21] P. Verma and R. W. Schafer, "Frequency estimation from waveforms using multi-layered neural networks," in *INTERSPEECH*, 2016, pp. 2165–2169.
- [22] G. Izacard, S. Mohan, and C. Fernandez-Granda, "Data-driven estimation of sinusoid frequencies," *Advances in Neural Information Process. Syst.*, vol. 32, 2019.

- [23] G. Izacard, B. Bernstein, and C. Fernandez-Granda, "A learning-based framework for line-spectra super-resolution," in *Int. Conf. on Acoust. Speech Signal Process. (ICASSP)*, IEEE, 2019, pp. 3632–3636.
- [24] Y. Xie, M. B. Wakin, and G. Tang, "Data-driven parameter estimation of contaminated damped exponentials," in *2021 55th Asilomar Conf. on Signals, Syst., and Computers*, IEEE, 2021, pp. 800–804.
- [25] P. Pan, Y. Zhang, Z. Deng, and W. Qi, "Deep learning-based 2-d frequency estimation of multiple sinusoidals," *IEEE Trans. Neural Networks Learn. Syst.*, vol. 33, no. 10, pp. 5429–5440, 2021.
- [26] P. Pan, Y. Zhang, Z. Deng, and G. Wu, "Complex-valued frequency estimation network and its applications to superresolution of radar range profiles," *IEEE Trans. Geosci. Remote Sens.*, vol. 60, pp. 1–12, 2021.
- [27] J. W. Smith and M. Torlak, "Frequency estimation using complex-valued shifted window transformer," *IEEE Geosci. Remote Sens. Lett.*, 2024.
- [28] B. Porat, *A course in digital signal processing*. John Wiley & Sons, Inc., 1996.
- [29] Y. Hua and T. K. Sarkar, "Matrix pencil method for estimating parameters of exponentially damped/undamped sinusoids in noise," *IEEE Trans. Acoust. Speech Signal Process.*, vol. 38, no. 5, pp. 814–824, 1990.
- [30] Y. Hua and T. K. Sarkar, "Matrix pencil method and its performance," in *Int. Conf. on Acoust. Speech Signal Process. (ICASSP)*, IEEE Computer Society, 1988, pp. 2476–2477.
- [31] T. K. Sarkar and O. Pereira, "Using the matrix pencil method to estimate the parameters of a sum of complex exponentials," *IEEE Antennas Propag. Mag.*, vol. 37, no. 1, pp. 48–55, 1995.
- [32] F. Hu, T. K. Sarkar, and Y. Hua, "Utilization of band-pass filtering for the matrix pencil method," *IEEE Trans. Signal Process.*, vol. 41, no. 1, pp. 442–442, 1993.
- [33] J. F. del Rio and T. K. Sarkar, "Comparison between the matrix pencil method and the fourier transform technique for high-resolution spectral estimation," *Digital Signal Process.*, vol. 6, no. 2, pp. 108–125, 1996.
- [34] P. J. Schmid, "Dynamic mode decomposition of numerical and experimental data," *J. Fluid Mech.*, vol. 656, pp. 5–28, 2010.
- [35] D. Rao, "Perturbation analysis of a svd based method for the harmonic retrieval problem," in *Int. Conf. on Acoust. Speech Signal Process. (ICASSP)*, IEEE, vol. 10, 1985, pp. 624–627.
- [36] Y. Hua and T. K. Sarkar, "Perturbation analysis of tk method for harmonic retrieval problems," *IEEE Trans. Acoust. Speech Signal Process.*, vol. 36, no. 2, pp. 228–240, 1988.
- [37] E.-H. Djermoune and M. Tomczak, "Perturbation analysis of subspace-based methods in estimating a damped complex exponential," *IEEE Trans. Signal Process.*, vol. 57, no. 11, pp. 4558–4563, 2009.
- [38] J. Laroche, "The use of the matrix pencil method for the spectrum analysis of musical signals," *The Journal of the Acoustical Society of America*, vol. 94, no. 4, pp. 1958–1965, 1993.
- [39] M. Bhuiyan, E. V. Malyarenko, M. A. Pantea, F. M. Seviaryn, and R. G. Maev, "Advantages and limitations of using matrix pencil method for the modal analysis of medical percussion signals," *IEEE Trans. Biomed. Eng.*, vol. 60, no. 2, pp. 417–426, 2012.
- [40] H. Yin, Z. Zhu, and F. Ding, "Model order determination using the hankel matrix of impulse responses," *Appl. Math. Lett.*, vol. 24, no. 5, pp. 797–802, 2011.
- [41] J. N. Kutz, S. L. Brunton, B. W. Brunton, and J. L. Proctor, *Dynamic mode decomposition: data-driven modeling of complex systems*. SIAM, 2016.
- [42] J. R. Magnus, "On differentiating eigenvalues and eigenvectors," *Econom. Theory*, vol. 1, no. 2, pp. 179–191, 1985.
- [43] E. Bronstein, A. Wiegner, D. Shilo, and R. Talmon, "The spatiotemporal coupling in delay-coordinates dynamic mode decomposition," *Chaos: An Interdisciplinary Journal of Nonlinear Science*, vol. 32, no. 12, p. 123 127, 2022.
- [44] O. Roy and M. Vetterli, "The effective rank: A measure of effective dimensionality," in *2007 15th European signal process. conf.*, IEEE, 2007, pp. 606–610.
- [45] S. Dharanipragada and K. Arun, "Resolution limits in signal recovery," *IEEE Trans. Signal Process.*, vol. 44, no. 3, pp. 546–561, 1996.
- [46] M. Shahram and P. Milanfar, "On the resolvability of sinusoids with nearby frequencies in the presence of noise," *IEEE Trans. Signal Process.*, vol. 53, no. 7, pp. 2579–2588, 2005.
- [47] A. Amar and A. J. Weiss, "Fundamental limitations on the resolution of deterministic signals," *IEEE Trans. Signal Process.*, vol. 56, no. 11, pp. 5309–5318, 2008.
- [48] R. Kumaresan and D. Tufts, "Estimating the parameters of exponentially damped sinusoids and pole-zero modeling in noise," *IEEE Trans. Acoust. Speech Signal Process.*, vol. 30, no. 6, pp. 833–840, 1982.
- [49] S.-Y. Kung, K. S. Arun, and D. B. Rao, "State-space and singular-value decomposition-based approximation methods for the harmonic retrieval problem," *JOSA*, vol. 73, no. 12, pp. 1799–1811, 1983.
- [50] D. S. Broomhead and G. P. King, "Extracting qualitative dynamics from experimental data," *Physica D*, vol. 20, no. 2-3, pp. 217–236, 1986.
- [51] J. B. Elsner and A. A. Tsonis, *Singular spectrum analysis: a new tool in time series analysis*. Springer Science & Business Media, 1996.
- [52] A. Barabell, "Improving the resolution performance of eigenstructure-based direction-finding algorithms," in *Int. Conf. on Acoust. Speech Signal Process. (ICASSP)*, IEEE, vol. 8, 1983, pp. 336–339.
- [53] A. Greenbaum, R.-c. Li, and M. L. Overton, "First-order perturbation theory for eigenvalues and eigenvectors," *SIAM Rev.*, vol. 62, no. 2, pp. 463–482, 2020.
- [54] A. Deif, "Rigorous perturbation bounds for eigenvalues and eigenvectors of a matrix," *J. Comput. Appl. Math.*, vol. 57, no. 3, pp. 403–412, 1995.

- [55] G. Stewart, "Matrix perturbation theory," *Computer Science and Scientific Computing/Academic Press, Inc*, 1990.
- [56] P.-Å. Wedin, "Perturbation theory for pseudo-inverses," *BIT Numer. Math.*, vol. 13, pp. 217–232, 1973.

## SUPPLEMENTARY MATERIAL

### APPENDIX A

#### SIMPLE EIGENVECTOR PERTURBATION

In this appendix, we derive a first-order approximation for a simple eigenvector under perturbation. Simple eigenvectors, associated with simple eigenvalues, are known to display stable behavior under perturbations [42], [53]. Following [42], let  $\mathbf{A} \in \mathbb{C}^{n \times n}$  be a complex square matrix, and let  $\mathbf{v}_i$  denote a simple right eigenvector of  $\mathbf{A}$  corresponding to a simple eigenvalue  $\lambda_i$ . For a perturbed matrix  $\mathbf{A} + \delta\mathbf{A}$ , the author established the existence of a complex function  $\lambda$  and a complex vector function  $\mathbf{v}$  defined for all  $\delta\mathbf{A}$  in a neighborhood of  $\mathbf{A}$ , satisfying  $\lambda(\mathbf{A}) = \lambda_i$ ,  $\mathbf{v}(\mathbf{A}) = \mathbf{v}_i$ , and  $(\mathbf{A} + \delta\mathbf{A})\mathbf{v} = \lambda\mathbf{v}$ . These functions are infinitely differentiable within this neighborhood, with their differentials at  $\mathbf{A}$  also provided. While the proof is clear and elegant, we seek an alternative proof that will provide additional insights into the neighborhood in which eigenvector perturbation can be characterized.

Our approach follows the technique outlined in [54, Theorem 4.1], which assumes that the matrix  $\mathbf{A}$  is non-defective, forming an eigenvector basis for  $\mathbb{C}^n$ . Let  $\mathbf{V}$  and  $\mathbf{U}$  denote the matrices of its right and left eigenvectors, respectively, where  $\mathbf{u}_k^H$  is the  $k$ -th row of  $\mathbf{U}^H$  and  $\mathbf{v}_i$  is the  $i$ -th column of  $\mathbf{V}$ . The following lemma characterizes the approximate behavior of  $\mathbf{v}_i$  under perturbation, provided that a delicate balance between perturbation and eigenvalue separation is maintained.

**Lemma 1.** *Let  $\mathbf{v}_i$  be a simple right eigenvector of a non-defective matrix  $\mathbf{A} \in \mathbb{C}^{n \times n}$ , and let  $\lambda_i$  be its associated to simple eigenvalue. Then there is a unique right eigenvector  $\tilde{\mathbf{v}}_i = \mathbf{v}_i + \delta\mathbf{v}_i$  of the matrix  $\mathbf{A} + \delta\mathbf{A}$  and a corresponding eigenvalue  $\tilde{\lambda}_i = \lambda_i + \delta\lambda_i$  such that  $\delta\lambda_i$  and  $\delta\mathbf{v}_i$  can be approximated to first order by*

$$\delta\lambda_i = \frac{\mathbf{u}_i^H \delta\mathbf{A} \mathbf{v}_i}{\mathbf{u}_i^H \mathbf{v}_i}, \quad (46)$$

$$\delta\mathbf{v}_i = \sum_{\substack{k=1 \\ k \neq i}}^n \frac{\mathbf{u}_k^H \delta\mathbf{A} \mathbf{v}_i}{\mathbf{u}_k^H \mathbf{v}_k (\tilde{\lambda}_i - \lambda_k)} \mathbf{v}_k. \quad (47)$$

Provided that

$$\rho(\mathbf{D}_i \mathbf{U}^H \delta\mathbf{A} \mathbf{V}) < 1, \quad (48)$$

and

$$\mathbf{u}_i^H \mathbf{v}_i = 1, \quad \mathbf{u}_i^H \tilde{\mathbf{v}}_i = 1, \quad (49)$$

where  $\rho(\cdot)$  is the spectral radius, and the matrix  $\mathbf{D}_i$  is a diagonal matrix defined by

$$\mathbf{D}_i = \text{diag} \left( \frac{1}{\mathbf{u}_1^H \mathbf{v}_1 (\tilde{\lambda}_i - \lambda_1)}, \dots, 0_i, \dots, \frac{1}{\mathbf{u}_n^H \mathbf{v}_n (\tilde{\lambda}_i - \lambda_n)} \right). \quad (50)$$

*Proof.* The fact that there is a unique perturbed eigenvalue  $\tilde{\lambda}_i$  such that

$$\delta\lambda_i = \frac{\mathbf{u}_i^H \delta\mathbf{A} \mathbf{v}_i}{\mathbf{u}_i^H \mathbf{v}_i} + O(\|\delta\mathbf{A}\|^2), \quad (51)$$

is provided in [55, chapter IV, Theorem 2.3]. Let  $\tilde{\mathbf{v}}_i$  be its corresponding perturbed eigenvector. The non-defectiveness of the matrix  $\mathbf{A}$  implies that we can expand  $\delta\mathbf{v}_i = \tilde{\mathbf{v}}_i - \mathbf{v}_i$  in the eigenvector basis of  $\mathbf{A}$  as:

$$\delta\mathbf{v}_i = \sum_{k=1}^n a_{ik} \mathbf{v}_k. \quad (52)$$

Left multiplying (52) by  $\mathbf{u}_i^H$  results in:

$$a_{ii} = \frac{\mathbf{u}_i^H \tilde{\mathbf{v}}_i - \mathbf{u}_i^H \mathbf{v}_i}{\mathbf{u}_i^H \mathbf{v}_i}. \quad (53)$$

It follows, by assumption (49), that  $a_{ii} = 0$ . Thus, (52) can be written as:

$$\delta\mathbf{v}_i = \sum_{\substack{k=1 \\ k \neq i}}^n a_{ik} \mathbf{v}_k. \quad (54)$$

It is noteworthy that as the matrix  $\mathbf{A}$  is non-defective, its right eigenvector matrix  $\mathbf{V}$ , is invertible. As eigenvectors are unique up to scalar multiplication, it follows that there exists a diagonal matrix  $\mathbf{C} = \text{diag}(c_1, \dots, c_n)$ , where  $\{c_k\}_{k=1}^n \neq 0$ , such that  $\mathbf{C}\mathbf{V}^{-1} = \mathbf{U}^H$  or equivalently  $\mathbf{C} = \mathbf{U}^H \mathbf{V}$ . Consequently, each element  $c_k$  can be expressed as  $c_k = \mathbf{u}_k^H \mathbf{v}_k$ , ensuring that all the terms involving the reciprocal of  $\mathbf{u}_i^H \mathbf{v}_i$  are well defined.

The perturbed eigenvalue problem can be stated as

$$(\mathbf{A} + \delta\mathbf{A})(\mathbf{v}_i + \delta\mathbf{v}_i) = (\lambda_i + \delta\lambda_i)(\mathbf{v}_i + \delta\mathbf{v}_i).$$

Left multiplying by  $\mathbf{u}_k^H$  for  $k \neq i$  and rearranging, we can express the vector of coefficients  $\mathbf{a}_i$ , from (54), by the following relation:

$$(\mathbf{I} - \mathbf{D}_i \mathbf{U}^H \delta\mathbf{A} \mathbf{T}) \mathbf{a}_i = \mathbf{D}_i \mathbf{U}^H \delta\mathbf{A} \mathbf{v}_i, \quad (55)$$

where the matrix  $\mathbf{D}_i$  is defined in (50).

By Assumption (48), the spectral radius  $\rho(\mathbf{D}_i \mathbf{U}^H \delta\mathbf{A} \mathbf{V}) < 1$ , and we can explicitly express the coefficients vector  $\mathbf{a}_i$  by inverting the matrix  $(\mathbf{I} - \mathbf{D}_i \mathbf{U}^H \delta\mathbf{A} \mathbf{V})$ . Finally, as  $\rho(\mathbf{D}_i \mathbf{U}^H \delta\mathbf{A} \mathbf{V}) < 1$ , using the Neumann series representation of the matrix  $(\mathbf{I} - \mathbf{D}_i \mathbf{U}^H \delta\mathbf{A} \mathbf{V})^{-1}$ , we get the following first-order approximation for the coefficients vector:

$$\mathbf{a}_i = \mathbf{D}_i \mathbf{U}^H \delta\mathbf{A} \mathbf{v}_i. \quad (56)$$

This leads us to the following expression for  $a_{ik}$ :

$$a_{ik} = \begin{cases} 0 & , \text{ if } k = i, \\ \frac{\mathbf{u}_k^H \delta\mathbf{A} \mathbf{v}_i}{\mathbf{u}_k^H \mathbf{v}_k (\tilde{\lambda}_i - \lambda_k)} & , \text{ otherwise} \end{cases} \quad (57)$$

which completes the proof.  $\square$

APPENDIX B  
EXTENDING THE MATRIX PENCIL THEOREM:  
ACCOUNTING FOR NOISE EFFECTS

In this section, we extend the MP theorem [29, Theorem 2.1] to the noisy case and analyze the noise-induced effects. By doing so, we bridge the gap between the existing theory, described in Section II-C, and practice, described in Section II-A.

**Theorem 1.** *Assume the underlying signal is given by (1). Let  $\mathbf{Y}_0$  and  $\mathbf{Y}_1$  be the Hankel matrices defined in (3). Then,  $\mathbf{Y}_0$  and  $\mathbf{Y}_1$  admit the following factorization:*

$$\mathbf{Y}_0 = \tilde{\mathbf{Z}}_L \tilde{\mathbf{B}} \tilde{\mathbf{Z}}_R, \quad (58)$$

$$\mathbf{Y}_1 = \tilde{\mathbf{Z}}_L \tilde{\mathbf{B}} \tilde{\mathbf{\Lambda}} \tilde{\mathbf{Z}}_R, \quad (59)$$

where

- 1) The diagonal matrix  $\tilde{\mathbf{\Lambda}}$  consists of the MP eigenvalues, acts as a forward propagation in time, and can be recast as:

$$\tilde{\mathbf{\Lambda}} = \begin{bmatrix} \tilde{\mathbf{Z}} & \mathbf{0} \\ \mathbf{0} & \tilde{\mathbf{0}} \end{bmatrix}_{L \times L}, \quad (60)$$

where

- a) The diagonal matrix  $\tilde{\mathbf{Z}} \in \mathbb{C}^{M \times M}$  comprises the signal-related eigenvalues.
- b) The diagonal matrix  $\tilde{\mathbf{0}} \in \mathbb{C}^{(L-M) \times (L-M)}$  consists of the noise-related eigenvalues.

- 2) The diagonal matrix  $\tilde{\mathbf{B}}$  can be cast as

$$\tilde{\mathbf{B}} = \begin{bmatrix} \mathbf{B} & \mathbf{0} \\ \mathbf{0} & \mathbf{I}_{L-M} \end{bmatrix}_{L \times L}, \quad (61)$$

where the diagonal matrix  $\mathbf{B} \in \mathbb{C}^{M \times M}$  consists of the signal amplitudes as defined in 18.

- 3)  $\tilde{\mathbf{Z}}_R$ , which is defined in (19) as the pseudo-inverse of the right eigenvector matrix of the noisy MP, can be recast as:

$$\tilde{\mathbf{Z}}_R = \begin{bmatrix} \mathbf{Z}_R + \mathbf{E}_R \\ \mathbf{C}_R \end{bmatrix}_{L \times L}, \quad (62)$$

where the top  $M$  rows of  $\tilde{\mathbf{Z}}_R$  are the sum of the Vandermonde matrix  $\mathbf{Z}_R$  and a noise-related component, denoted by  $\mathbf{E}_R$ . The remaining  $L - M$  rows are noise-related spurious rows, denoted by  $\mathbf{C}_R$ .

- 4)  $\tilde{\mathbf{Z}}_L$ , which is defined in (20) as the pseudo-inverse of the left eigenvector matrix of the noisy MP, can be recast as

$$\tilde{\mathbf{Z}}_L = [\mathbf{Z}_L + \mathbf{E}_L, \mathbf{C}_L]_{(N-L) \times L}, \quad (63)$$

where the leftmost  $M$  columns of  $\tilde{\mathbf{Z}}_L$  are the sum of the Vandermonde matrix  $\mathbf{Z}_L$  and a noise-related component, denoted by  $\mathbf{E}_L$ . The remaining  $L - M$  columns are noise-related spurious columns, denoted by  $\mathbf{C}_L$ .

*Proof.* Using the definition of  $\tilde{\mathbf{Z}}_R^\dagger$  and  $\tilde{\mathbf{Z}}_L^\dagger$  from (21) and (22), and the SVD of  $\mathbf{Y}_0 = \mathbf{U}\mathbf{\Sigma}\mathbf{V}^H$  from (4), it is easy to verify that  $\tilde{\mathbf{Z}}_L^\dagger \mathbf{Y}_0 \tilde{\mathbf{Z}}_R^\dagger = \mathbf{I}_L$ , and  $\tilde{\mathbf{Z}}_L^\dagger \mathbf{Y}_1 \tilde{\mathbf{Z}}_R^\dagger = \mathbf{\Lambda}$ , where  $\mathbf{I}_L$  is the

$L \times L$  identity matrix. From these equalities we find a new representation for the noisy Hankel matrices:

$$\mathbf{Y}_0 = \tilde{\mathbf{Z}}_L \tilde{\mathbf{Z}}_R, \quad (64)$$

$$\mathbf{Y}_1 = \tilde{\mathbf{Z}}_L \mathbf{\Lambda} \tilde{\mathbf{Z}}_R. \quad (65)$$

By employing the Vandermonde factorization of  $\mathbf{X}_0$ , we can express the Hankel matrix  $\mathbf{Y}_0$  as

$$\mathbf{Y}_0 = \mathbf{X}_0 + \mathbf{W}_0 = \mathbf{Z}_L \mathbf{B} \mathbf{Z}_R + \mathbf{W}_0. \quad (66)$$

Let us re-frame equation (66) as follows:

$$\mathbf{Y}_0 = (\mathbf{Z}_L \mathbf{B}^{\frac{1}{2}})(\mathbf{B}^{\frac{1}{2}} \mathbf{Z}_R) + \mathbf{W}_0, \quad (67)$$

as this formulation will prove to be useful in subsequent discussions. Combining (64) and (67), we get:

$$\tilde{\mathbf{Z}}_L = (\mathbf{Z}_L \mathbf{B}^{\frac{1}{2}})(\mathbf{B}^{\frac{1}{2}} \mathbf{Z}_R) \tilde{\mathbf{Z}}_R^\dagger + \mathbf{W}_0 \tilde{\mathbf{Z}}_R^\dagger. \quad (68)$$

Now, let us analyze the term  $\mathbf{B}^{\frac{1}{2}} \mathbf{Z}_R \tilde{\mathbf{Z}}_R^\dagger$ . As established in [29, Theorem 2.1], the columns of  $\mathbf{Z}_R^\dagger$  (and hence the columns of  $\mathbf{Z}_R^\dagger \mathbf{B}^{-\frac{1}{2}}$ ) are right eigenvectors of the noiseless MP ( $\mathbf{X}_0, \mathbf{X}_1$ ), or equivalently, right simple eigenvectors of  $\mathbf{X}_0^\dagger \mathbf{X}_1$  corresponding to its non-zero and simple eigenvalues. Furthermore, by definition, the columns of  $\tilde{\mathbf{Z}}_R^\dagger$  are right eigenvectors of the noisy MP  $\mathbf{Y}_1 - \lambda \mathbf{Y}_0$ , or equivalently, right eigenvectors of  $\mathbf{Y}_0^\dagger \mathbf{Y}_1$ .

As each  $\{z_i\}_{i=1}^M$  is a simple eigenvalue of  $\mathbf{X}_0^\dagger \mathbf{X}_1$ , and  $\mathbf{Y}_0^\dagger \mathbf{Y}_1$  is a perturbation of  $\mathbf{X}_0^\dagger \mathbf{X}_1$ , according to Theorem 2.3, chapter IV in [55], we can uniquely match each simple eigenvector of  $\mathbf{X}_0^\dagger \mathbf{X}_1$  with a simple eigenvector of  $\mathbf{Y}_0^\dagger \mathbf{Y}_1$ <sup>4</sup>. Without loss of generality, let the leftmost  $M$  columns of  $\tilde{\mathbf{Z}}_R^\dagger$  consist of these perturbed eigenvectors, which are the  $M$  columns of  $\mathbf{Z}_R^\dagger$ . Consequently, we can express this relationship as follows:

$$\tilde{\mathbf{Z}}_R^\dagger = [\mathbf{Z}_R^\dagger \mathbf{B}^{-\frac{1}{2}} + \delta \mathbf{Z}_R^\dagger, \mathbf{C}_1]_{L \times L} \quad (69)$$

where  $\mathbf{C}_1 \in \mathbb{C}^{L \times (L-M)}$  contains the remaining  $L - M$  eigenvectors of  $\mathbf{Y}_0^\dagger \mathbf{Y}_1$  and  $\delta \mathbf{Z}_R^\dagger \in \mathbb{C}^{L \times M}$  represents the additive discrepancy in the scaled, right eigenvectors matrix  $\mathbf{Z}_R^\dagger \mathbf{B}^{-\frac{1}{2}}$  due to the perturbation of the noiseless matrix  $\mathbf{X}_0^\dagger \mathbf{X}_1$ . Substituting (69) into (68), we get the following structure of the left mode:

$$\tilde{\mathbf{Z}}_L = (\mathbf{Z}_L \mathbf{B}^{\frac{1}{2}})(\mathbf{B}^{\frac{1}{2}} \mathbf{Z}_R) [\mathbf{Z}_R^\dagger \mathbf{B}^{-\frac{1}{2}} + \delta \mathbf{Z}_R^\dagger, \mathbf{C}_1] + \mathbf{W}_0 [\mathbf{Z}_R^\dagger \mathbf{B}^{-\frac{1}{2}} + \delta \mathbf{Z}_R^\dagger, \mathbf{C}_1]. \quad (70)$$

Which can be re-arranged to the following form:

$$\tilde{\mathbf{Z}}_L = [\mathbf{Z}_L \mathbf{B}^{\frac{1}{2}} + \mathbf{X}_0 \delta \mathbf{Z}_R^\dagger + \mathbf{W}_0 \mathbf{Z}_R^\dagger \mathbf{B}^{-\frac{1}{2}} + \mathbf{W}_0 \delta \mathbf{Z}_R^\dagger, \mathbf{Y}_0 \mathbf{C}_1]. \quad (71)$$

<sup>4</sup>Theorem 2.3, chapter IV in [55] guarantees that there is a unique perturbed eigenvalue  $\tilde{z}_i$ , such that

$$\tilde{z}_i = z_i + \frac{\mathbf{p}_i'^* \delta(\mathbf{X}_0^\dagger \mathbf{X}_1) \mathbf{q}_i'}{\mathbf{p}_i'^* \mathbf{q}_i'} + O(\|\delta(\mathbf{X}_0^\dagger \mathbf{X}_1)\|^2)$$

where  $\mathbf{q}_i'$  and  $\mathbf{p}_i'^*$  are the corresponding right and left eigenvectors of the matrix  $\mathbf{X}_0^\dagger \mathbf{X}_1$  and  $\mathbf{Y}_0^\dagger \mathbf{Y}_1 = \mathbf{X}_0^\dagger \mathbf{X}_1 + \delta(\mathbf{X}_0^\dagger \mathbf{X}_1)$ .

To obtain the desired normalized form, define the diagonal matrix

$$\tilde{\mathbf{B}} = \begin{bmatrix} \mathbf{B} & 0 \\ 0 & \mathbf{I}_{L-M} \end{bmatrix}_{L \times L},$$

to get

$$\tilde{\mathbf{Z}}_L \tilde{\mathbf{B}}^{-\frac{1}{2}} = [\mathbf{Z}_L + \mathbf{E}_L, \mathbf{C}_L], \quad (72)$$

where the noise-related component  $\mathbf{E}_L$  and the spurious matrix  $\mathbf{C}_L$  are defined by

$$\mathbf{E}_L = \mathbf{X}_0 \delta \mathbf{Z}_R^\dagger \mathbf{B}^{-\frac{1}{2}} + \mathbf{W}_0 \mathbf{Z}_R^\dagger \mathbf{B}^{-1} + \mathbf{W}_0 \delta \mathbf{Z}_R^\dagger \mathbf{B}^{-\frac{1}{2}}, \quad (73)$$

$$\mathbf{C}_L = \mathbf{Y}_0 \mathbf{C}_1. \quad (74)$$

For simplicity, we maintain the notation  $\tilde{\mathbf{Z}}_L$  for the normalized form, i.e.,  $\tilde{\mathbf{Z}}_L = \tilde{\mathbf{Z}}_L \tilde{\mathbf{B}}^{-\frac{1}{2}}$ .

Following the same technique as in (69), the left eigenvectors matrix can be recast as:

$$\tilde{\mathbf{Z}}_L^\dagger = \begin{bmatrix} \mathbf{B}^{-\frac{1}{2}} \mathbf{Z}_L^\dagger + \delta \mathbf{Z}_L^\dagger \\ \mathbf{C}_2 \end{bmatrix}_{L \times (N-L)}, \quad (75)$$

where  $\mathbf{C}_2 \in \mathbb{C}^{(L-M) \times (N-L)}$  and  $\delta \mathbf{Z}_L^\dagger \in \mathbb{C}^{M \times (N-L)}$ , to obtain the desired structure of:

$$\tilde{\mathbf{B}}^{-\frac{1}{2}} \tilde{\mathbf{Z}}_R = \begin{bmatrix} \mathbf{Z}_R + \mathbf{E}_R \\ \mathbf{C}_R \end{bmatrix}, \quad (76)$$

where,

$$\mathbf{E}_R = \mathbf{B}^{-\frac{1}{2}} \delta \mathbf{Z}_L^\dagger \mathbf{X}_0 + \mathbf{B}^{-1} \mathbf{Z}_L^\dagger \mathbf{W}_0 + \mathbf{B}^{-\frac{1}{2}} \delta \mathbf{Z}_L^\dagger \mathbf{W}_0, \quad (77)$$

$$\mathbf{C}_R = \mathbf{C}_2 \mathbf{Y}_0. \quad (78)$$

For simplicity, we maintain the notation  $\tilde{\mathbf{Z}}_R$  for the normalized form, i.e.,  $\tilde{\mathbf{Z}}_R = \tilde{\mathbf{B}}^{-\frac{1}{2}} \mathbf{Z}_R$ . Combining the normalized forms of  $\tilde{\mathbf{Z}}_L$  and  $\tilde{\mathbf{Z}}_R$  with the decomposition of the Hankel matrices  $\mathbf{Y}_0$  and  $\mathbf{Y}_1$  from (64) and (65) leads to the desired normalized factorization of  $\mathbf{Y}_0 = \tilde{\mathbf{Z}}_L \tilde{\mathbf{B}} \tilde{\mathbf{Z}}_R$  and  $\mathbf{Y}_1 = \tilde{\mathbf{Z}}_L \tilde{\mathbf{B}} \tilde{\mathbf{\Lambda}} \tilde{\mathbf{Z}}_R$ .

The partitioning of  $\tilde{\mathbf{\Lambda}}$  to signal-related and noise-related components is derived from the assumption on the order of vectors in  $\tilde{\mathbf{Z}}_R^\dagger$  and  $\tilde{\mathbf{Z}}_L^\dagger$ . We assumed, without loss of generality, that the leftmost  $M$  columns of  $\tilde{\mathbf{Z}}_R^\dagger$  are the perturbed versions of the  $M$  simple right eigenvectors of  $\mathbf{X}_0^\dagger \mathbf{X}_1$  corresponding to the signal poles. A parallel assumption is made on the top  $M$  rows of  $\tilde{\mathbf{Z}}_L^\dagger$ . Such ordering, of the right and left eigenvectors of the matrix  $\mathbf{X}_0^\dagger \mathbf{X}_1$ , induces the same ordering on the corresponding eigenvalues matrix  $\tilde{\mathbf{\Lambda}}$ . Hence the decomposition of  $\tilde{\mathbf{\Lambda}}$  in (60). This completes the proof.  $\square$

## APPENDIX C PROOF OF PROPOSITION 2

*Proof.* The left additive error term was shown to be:

$$\mathbf{E}_L = \mathbf{X}_0 \delta \mathbf{Z}_R^\dagger \mathbf{B}^{-\frac{1}{2}} + \mathbf{W}_0 \mathbf{Z}_R^\dagger \mathbf{B}^{-1} + \mathbf{W}_0 \delta \mathbf{Z}_R^\dagger \mathbf{B}^{-\frac{1}{2}}. \quad (79)$$

We begin by examining the term  $\delta \mathbf{Z}_R^\dagger \in \mathbb{C}^{L \times M}$ , which represents the additive discrepancy in the scaled right eigenvectors matrix of the noiseless MP pair  $(\mathbf{X}_0, \mathbf{X}_1)$ . Recalling that the matrix  $\mathbf{X}_0^\dagger \mathbf{X}_1$  is non-defective, with its complete set of  $L$  independent right and left eigenvectors denoted as  $\{\mathbf{q}'_k\}_{k=1}^L$

and  $\{\mathbf{p}'_k\}_{k=1}^L$ , respectively. Let  $\{\delta \mathbf{q}_i\}_{i=1}^M$  represent the  $i$ -th column of  $\delta \mathbf{Z}_R^\dagger$ . We can express  $\delta \mathbf{q}_i$  as:

$$\delta \mathbf{q}_i = \sum_{k=1}^L a_{ik} \mathbf{q}'_k = \sum_{k=1}^M a_{ik} \mathbf{q}'_k + \sum_{k=M+1}^L a_{ik} \mathbf{q}'_k. \quad (80)$$

Through the Vandermonde factorization of  $\mathbf{X}_0$  and  $\mathbf{X}_1$ , we get  $\mathbf{X}_0^\dagger \mathbf{X}_1 = \mathbf{Z}_R^\dagger \mathbf{Z} \mathbf{Z}_R$ . Consequently, for  $1 \leq k \leq M$   $\mathbf{q}'_k$  is the  $k$ -th column of  $\mathbf{Z}_R^\dagger$ ,  $\mathbf{p}'_k{}^H$  is the  $k$ -th row of  $\mathbf{Z}_R$  and  $\mathbf{p}'_k{}^H \mathbf{q}'_k = 1$ . It follows from Theorem [29, Theorem 2.1] that  $\mathbf{q}'_k = \mathbf{q}_k$  for  $1 \leq k \leq M$ . However, for  $M < k \leq L$ ,  $\mathbf{q}'_k$  lies in the null space of  $\mathbf{X}_0^\dagger \mathbf{X}_1$ , implying  $\mathbf{X}_0 \mathbf{q}'_k = 0$ . Substituting this decomposition back into (79), we obtain:

$$\mathbf{E}_L^i = \frac{\mathbf{X}_0}{\sqrt{b_i}} \sum_{k=1}^M a_{ik} \mathbf{q}_k + \frac{\mathbf{W}_0 \mathbf{q}_i}{b_i} + \frac{\mathbf{W}_0}{\sqrt{b_i}} \sum_{k=M+1}^L a_{ik} \mathbf{q}'_k. \quad (81)$$

Using again the Vandermonde factorization of  $\mathbf{X}_0 = \mathbf{Z}_L \mathbf{B} \mathbf{Z}_R$  and the fact that  $\mathbf{q}_k$  is the  $k$ -th column of  $\mathbf{Z}_R^\dagger$ , we get:

$$\mathbf{E}_L^i = \sum_{k=1}^M \frac{a_{ik} b_k}{\sqrt{b_i}} \begin{bmatrix} 1 \\ z_k \\ \vdots \\ z_k^{N-L-1} \end{bmatrix} + \frac{\mathbf{W}_0 \mathbf{q}_i}{b_i} + \frac{\mathbf{W}_0}{\sqrt{b_i}} \sum_{k=M+1}^L a_{ik} \mathbf{q}'_k. \quad (82)$$

We now turn to get a first-order approximation of the coefficients  $a_{ik}$  using Lemma 1 applied to the matrix  $\mathbf{X}_0^\dagger \mathbf{X}_1$ , its perturbation  $\mathbf{Y}_0^\dagger \mathbf{Y}_1 = \mathbf{X}_0^\dagger \mathbf{X}_1 + \delta(\mathbf{X}_0^\dagger \mathbf{X}_1)$ , and to the simple, scaled, right eigenvectors  $\mathbf{Z}_R^\dagger \mathbf{B}^{-\frac{1}{2}}$  of  $\mathbf{X}_0^\dagger \mathbf{X}_1$ .

Lemma 1 assumes a specific normalization for the right, simple eigenvectors, and their perturbation. As noted above, for each simple eigenvector  $\{\mathbf{q}'_k\}_{k=1}^M$  it holds that  $\mathbf{p}'_k{}^H \mathbf{q}'_k = 1$ . Additionally, by our Assumption 1, we have  $\mathbf{p}'_k{}^H \tilde{\mathbf{q}}'_k = 1$ . Finally, by Assumption (27),  $\rho(\mathbf{D}_i \mathbf{T}_L \delta(\mathbf{X}_0^\dagger \mathbf{X}_1) \mathbf{T}_R) < 1$ , and hence we can apply Lemma 1 to get the first order approximation of the coefficients  $a_{ik}$ :

$$a_{ik} = \begin{cases} 0 & , k = i \\ \frac{\mathbf{p}'_k{}^H \delta(\mathbf{X}_0^\dagger \mathbf{X}_1) \mathbf{q}'_i}{\sqrt{b_i} (\tilde{\lambda}_i - \lambda_k)} & , \text{otherwise.} \end{cases}$$

Note that  $\lambda_k$  are the eigenvalues of  $\mathbf{X}_0^\dagger \mathbf{X}_1$ , which are assumed to be indexed such that:

$$\lambda_k = \begin{cases} z_k, & \text{if } 1 \leq k \leq M \\ 0, & \text{otherwise,} \end{cases}$$

and  $\tilde{\lambda}_i$  is the unique perturbation of  $\lambda_i$  as described in Lemma 1. As noted above,  $\mathbf{q}'_i = \mathbf{q}_i$  for  $1 \leq i \leq M$  and hence:

$$a_{ik} = \begin{cases} 0 & , k = i \\ \frac{\mathbf{p}'_k{}^H \delta(\mathbf{X}_0^\dagger \mathbf{X}_1) \mathbf{q}_i}{\sqrt{b_i} (\tilde{\lambda}_i - \lambda_k)} & , \text{otherwise.} \end{cases}$$

Following the approach presented in [29, section IV], the term  $\mathbf{p}'_k{}^H \delta(\mathbf{X}_0^\dagger \mathbf{X}_1) \mathbf{q}_i$ , can be approximated to first order by

$$\mathbf{p}'_k{}^H \delta(\mathbf{X}_0^\dagger \mathbf{X}_1) \mathbf{q}_i = \mathbf{p}'_k{}^H (\delta(\mathbf{Y}_0^\dagger) \mathbf{X}_1) \mathbf{q}_i + \mathbf{p}'_k{}^H (\mathbf{X}_0^\dagger \mathbf{W}_1) \mathbf{q}_i. \quad (83)$$

For  $1 \leq k \leq M$  it is also shown in [29] that a first order approximation of (83) is given by:

$$\mathbf{p}'_k{}^H \delta(\mathbf{X}_0^\dagger \mathbf{X}_1) \mathbf{q}_i = \frac{\mathbf{p}'_k{}^H (\mathbf{W}_1 - z_i \mathbf{W}_0) \mathbf{q}_i}{b_k}, \quad (84)$$

where  $\mathbf{p}_k^H$  is the  $k$ -th row of  $\mathbf{Z}_L^\dagger$ , as described in [29, Theorem 2.1]. On the other hand, for  $M < k \leq L$ , the rightmost term of (83) annihilates and we are left with  $\mathbf{p}_k^{iH}(\delta(\mathbf{Y}_0^\dagger)\mathbf{X}_1)\mathbf{q}_i$ . Using the decomposition theorem for pseudo-inverses, given in [56], we can write:

$$\begin{aligned} \delta\mathbf{Y}_0^\dagger &= -\mathbf{Y}_0^\dagger\mathbf{W}_0\mathbf{X}_0^\dagger + (\mathbf{Y}_0^H\mathbf{Y}_0)^\dagger\mathbf{W}_0^H P_{N(\mathbf{X}_0^H)} \\ &\quad + P_{N(\mathbf{Y}_0)}\mathbf{W}_0^H(\mathbf{X}_0\mathbf{X}_0^H)^\dagger, \end{aligned} \quad (85)$$

where  $P_X$  is the orthogonal projection onto a subspace  $X$ .

Combining (84) and (85) back into (82), a first order approximation of  $\mathbf{E}_L^i$  is given by:

$$\mathbf{E}_L^i = \sum_{\substack{k=1 \\ k \neq i}}^M \frac{\mathbf{p}_k^H(\mathbf{W}_1 - z_i\mathbf{W}_0)\mathbf{q}_i}{b_i(\tilde{\lambda}_i - z_k)} \begin{bmatrix} 1 \\ z_k \\ \vdots \\ z_k^{N-L-1} \end{bmatrix} + \frac{\mathbf{W}_0\mathbf{q}_i}{b_i}. \quad (86)$$

**Remark 6.** Assumption (27) intricately implies a delicate balance between the  $i$ -th pole separation and perturbation. Two observations support this. (i) Recognizing that matrix  $\mathbf{D}_i$  contains information about the separation and perturbation of the  $i$ -th pole as:

$$(\tilde{\lambda}_i - \lambda_k) = (\tilde{\lambda}_i - \lambda_i) - (\lambda_k - \lambda_i).$$

(ii) Referring to [55, Theorem 3.3, Chapter IV], the following inequality holds:

$$\max_i \min_k |\tilde{\lambda}_i - \lambda_k| \leq \left\| \mathbf{T}_R^{-1} \delta(\mathbf{X}_0^\dagger \mathbf{X}_1) \mathbf{T}_R \right\|, \quad (87)$$

and hence the inequality:

$$1 \leq \frac{\left\| \mathbf{T}_R^{-1} \delta(\mathbf{X}_0^\dagger \mathbf{X}_1) \mathbf{T}_R \right\|}{\min_k |\tilde{\lambda}_i - \lambda_k|} \quad (88)$$

holds for all indices  $1 \leq i \leq M$ .

Equations (27) and (88) are related through the connection between the spectral radius and spectral norm, but differ in two aspects: (i) the  $i$ -th coordinate of the matrix  $\mathbf{D}_i$  is set to zero<sup>5</sup>, and (ii) the matrix norm is used, providing a natural upper bound on the spectral radius.

#### APPENDIX D

##### PROOF OF PROPOSITION 3

*Proof.* Recall that:

$$\gamma_{i,m} = \frac{\mathbf{u}_m^T \mathbf{Q}_i \mathbf{w}}{(\tilde{\lambda}_i - z_m)b_i}, \quad \xi_i = \frac{\mathbf{I}_0 \mathbf{Q}_i \mathbf{w}}{b_i}, \quad (89)$$

and for simplicity, denote:

$$\bar{\gamma}_{i,m} = \frac{\mathbf{u}_m^T \mathbf{Q}_i \mathbf{w}}{b_i}. \quad (90)$$

Equation (89) shows that  $\bar{\gamma}_{i,m}$  and the entries of  $\xi_i$  are a linear combination of the complex, i.i.d Gaussian random variables  $\{\mathbf{w}(n)\}_{n=1}^n$  with zero mean and variance  $\sigma_w^2$ . Hence,  $\bar{\gamma}_{i,m}$  and the entries of  $\xi_i$  are also complex, Gaussian random

variables with zero mean. Inspecting the circular structure of the matrix  $\mathbf{Q}_i$ , we can recast the term  $\mathbf{u}_m \mathbf{Q}_i$  as the convolution of the vectors  $\mathbf{q}_i$  and  $\mathbf{u}_m$ . Using (90), we derive the following statistics of  $\bar{\gamma}_{i,m}$ :

$$\mathbb{E}[\bar{\gamma}_{i,m}] = 0, \quad (91)$$

$$\text{Var}(\bar{\gamma}_{i,m}) = \frac{\|\mathbf{u}_m * \mathbf{q}_i\|_2^2}{\text{SNR}_i}. \quad (92)$$

It is worth recalling that the vector  $\mathbf{u}_m$  was defined in (32) by

$$\mathbf{u}_m^T = [0, \mathbf{p}_m^H] - z_i [\mathbf{p}_m^H, 0],$$

where  $\mathbf{p}_m^H$  and  $\mathbf{q}_i$  depend solely on the signal poles and the parameters  $N$  and  $L$ , as they are also given by the  $m$ -th row of  $\mathbf{Z}_L^\dagger$  and  $i$ -th column of  $\mathbf{Z}_R^\dagger$ , respectively.

Since  $\bar{\gamma}_{i,m}$  is a complex Gaussian random variable,  $|\bar{\gamma}_{i,m}|$  follows a Rayleigh distribution with scale parameter  $\sigma_{\bar{\gamma}_{i,m}} = \text{var}(\bar{\gamma}_{i,m})$ . By setting  $t = \sigma_{\bar{\gamma}_{i,m}} \sqrt{2 \log(\frac{1}{\varepsilon})}$ , we ensure that  $|\bar{\gamma}_{i,m}| \leq t$  with a probability of at least  $1 - \varepsilon$ . Utilizing (92), it follows that:

$$|\bar{\gamma}_{i,m}| \leq \sqrt{\frac{2 \log(\frac{1}{\varepsilon})}{\text{SNR}_i}} \|\mathbf{u}_m * \mathbf{q}_i\|_2,$$

with a probability of at least  $1 - \varepsilon$ .

To derive the bound on  $\gamma_{i,m}$ , we use our assumption that  $|z_i - z_m| \geq 2|\delta z_i|$  for  $m \neq i$ , to get:

$$|\tilde{\lambda}_i - z_m| = |z_i + \delta z_i - z_m| \geq |z_i - z_m| - |\delta z_i| \geq \frac{|z_i - z_m|}{2}.$$

Finally, we derive that:

$$|\gamma_{i,m}| \leq 2 \sqrt{\frac{2 \log(\frac{1}{\varepsilon})}{\text{SNR}_i}} \frac{\|\mathbf{u}_m * \mathbf{q}_i\|_2}{|z_i - z_m|},$$

with a probability of at least  $1 - \varepsilon$ .

The entries of  $\xi_i$  can be bounded similarly. Writing the  $k$ -th entry of  $\xi_i$  by  $\xi_i(k) = \mathbf{e}_k^T \xi_i$ , where  $\mathbf{e}_k$  is the  $k$ -th standard unit vector we get:

$$\xi_i(k) = \frac{\mathbf{e}_k^T \mathbf{I}_0 \mathbf{Q}_i \mathbf{w}}{b_i},$$

and we derive the following statistics of  $\xi_i(k)$ :

$$\mathbb{E}[\xi_i(k)] = 0, \quad (93)$$

$$\text{Var}(\xi_i(k)) = \frac{\|\mathbf{e}_k^T \mathbf{I}_0 \mathbf{Q}_i\|_2^2}{\text{SNR}_i}. \quad (94)$$

Re-casting  $\mathbf{e}_k^T \mathbf{I}_0 \mathbf{Q}_i$  as a convolution of two vectors and using Young's convolution inequality, we achieve the following bound:

$$\text{Var}(\xi_i(k)) \leq \frac{1}{\text{SNR}_i}. \quad (95)$$

It follows that:

$$|\xi_i(k)| \leq \sqrt{\frac{2 \log(\frac{1}{\varepsilon})}{\text{SNR}_i}},$$

with a probability of at least  $1 - \varepsilon$ . □

<sup>5</sup>This motivates the eigenvector normalization in Assumption 1.

APPENDIX E  
PROOF OF PROPOSITION 4

*Proof.* By definition (31), the entries of  $\xi_i$  are Gaussian with zero mean and variance smaller than  $\frac{1}{\text{SNR}_i}$  (see the proof of Proposition 3). It follows that the entries of  $\mathcal{F}(\xi_i)$  are also complex Gaussian with zero mean and variance smaller than  $\frac{N-L}{\text{SNR}_i}$ . Consequently,  $|\mathcal{F}(\xi_i)[k]|$  follows Rayleigh distribution, and we obtain the following bound:

$$|\mathcal{F}(\xi_i)[k]| \leq \sqrt{\frac{2\log(\frac{1}{\varepsilon})(N-L)}{\text{SNR}_i}}, \quad (96)$$

with a probability of at least  $1 - \varepsilon$ . Hence, if the  $\text{SNR}_i$  is sufficiently high:

$$\frac{2\log(\frac{1}{\varepsilon})}{N-L} \ll \text{SNR}_i,$$

the condition on the DFT of the noise factor in (37) is met, i.e.,

$$|\mathcal{F}(\xi_i)[k]| \ll N - L,$$

with a probability of at least  $1 - \varepsilon$ .  $\square$

APPENDIX F  
LOCAL PERSPECTIVES FOR SIGNAL MODES DETECTION

To exploit the obscure multiplicative Vandermonde structure in (30), we could examine the following ratio between consecutive entries of  $\tilde{\mathbf{Z}}_L^i$ :

$$\hat{z}_i(k) := \frac{\tilde{\mathbf{Z}}_L^i(k+1)}{\tilde{\mathbf{Z}}_L^i(k)} = \frac{z_i^k + \mathbf{E}_L^i(k+1)}{z_i^{k-1} + \mathbf{E}_L^i(k)}, \quad (97)$$

for  $1 \leq k \leq N - L - 1$ .

Informally, when  $|\mathbf{E}_L^i(k)|$  and  $|\mathbf{E}_L^i(k+1)|$  are sufficiently small, the ratio  $\hat{z}_i(k)$  in (97) can be approximated by:

$$\begin{aligned} \hat{z}_i(k) &= \frac{z_i^k + \mathbf{E}_L^i(k+1)}{z_i^{k-1} + \mathbf{E}_L^i(k)} = z_i \left( \frac{1 + \frac{\mathbf{E}_L^i(k+1)}{z_i^k}}{1 + \frac{\mathbf{E}_L^i(k)}{z_i^{k-1}}} \right) \\ &\approx z_i \left( 1 + \frac{\mathbf{E}_L^i(k+1)}{z_i^k} - \frac{\mathbf{E}_L^i(k)}{z_i^{k-1}} \right) \end{aligned} \quad (98)$$

using standard linear approximation techniques.

Equation (98) shows that the ratios between consecutive entries of the  $i$ -th signal mode are centered around a *constant* value, which is the  $i$ -th signal pole  $z_i$ . In the context of dynamic mode decomposition (DMD) for data-driven dynamical systems analysis, Bronstein et al. [43] proposed to use the features:  $\epsilon_i = |\tilde{\lambda}_i - \mu_{\tilde{z}_i}|$ , which can now be supported by the first-order approximation of  $\tilde{\lambda}_i$ , given by [29]:

$$\tilde{\lambda}_i \cong z_i + \frac{\mathbf{u}_m \mathbf{Q}_i \mathbf{w}}{b_i}.$$

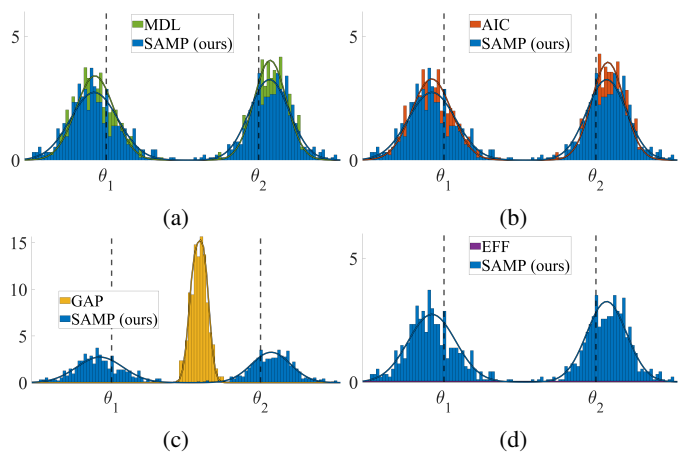


Fig. 8: Estimated frequencies distribution of all competing methods in the damped case, at  $\text{SNR}_{\text{dB}}$  level of 10 dB.

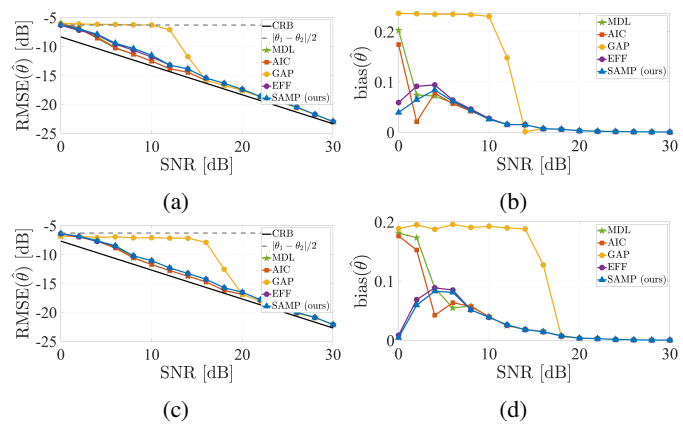


Fig. 9:  $\text{RMSE}(\hat{\theta}_1)$  and  $|\text{bias}(\hat{\theta}_1)|$  versus the  $\text{SNR}_{\text{dB}}$ . The undamped case is presented in (a) and (b). The damped case is presented in (c) and (d). The  $\text{SNR}_{\text{dB}}$  level is 10 dB.

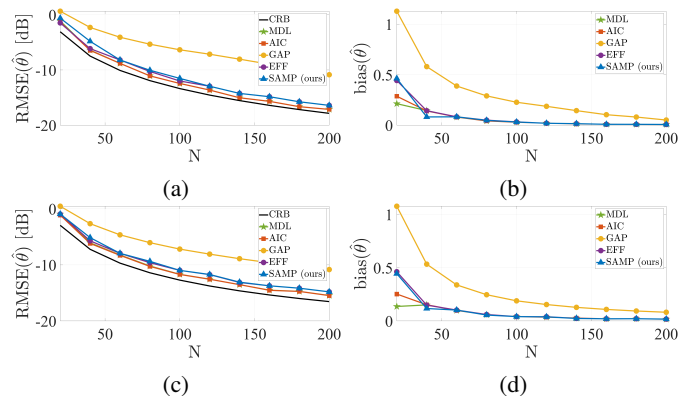


Fig. 10:  $\text{RMSE}(\hat{\theta}_1)$  and  $|\text{bias}(\hat{\theta}_1)|$  versus the number of samples. The undamped case is presented in (a) and (b). The damped case is presented in (c) and (d). The  $\text{SNR}_{\text{dB}}$  level is 10 dB.

APPENDIX G  
ADDITIONAL NUMERICAL RESULTS

In this appendix, we provide the complementary results for Section VII. Fig. 8 is the same as Fig. 4, but displays the

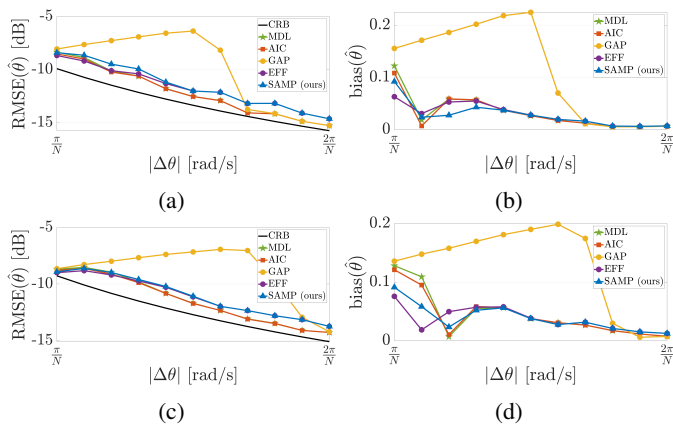


Fig. 11:  $\text{RMSE}(\hat{\theta}_1)$  and  $|\text{bias}(\hat{\theta}_1)|$  versus the frequencies distance. The undamped case is presented in (a) and (b). The damped case is presented in (c) and (d). The  $\text{SNR}_{\text{dB}}$  level is 10 dB.

estimated frequency distribution for the damped case, along with their estimated PDFs. Fig. 9 is complementary for Fig. 5, and displays the  $\text{RMSE}(\hat{\theta}_1)$  in dB and empirical bias of the estimate  $\hat{\theta}_1$  in absolute value versus the SNR. Fig. 10 is the same as Fig. 5, but display the  $\text{RMSE}(\hat{\theta}_1)$  in dB and empirical bias in absolute value versus the number of samples. Fig. 11 is the same as Fig. 5, but display the  $\text{RMSE}(\hat{\theta}_1)$  in dB and empirical bias in absolute value versus the frequencies distance.